POLITECNICO
MILANO 1863

SCUOLA DI INGEGNERIA INDUSTRIALE
E DELL'INFORMAZIONE

# Acceleration by the ARC Approach of Reactive Flow Simulations in CFD Aerospace Applications

Tesi di Laurea Magistrale in
Aeronautical Engineering - Ingegneria Aeronautica

**Giovanni Sacchini, 10482847**

**Advisor:**
Prof. Federico Piscaglia

**Academic year:**
2021-2022

**Abstract:** The industrial community has recently risen the interest in the development and optimization of fast and reliable algorithms for Computational Fluid Dynamic (CFD) simulations. This work investigates the use of the Analitically Reduced Chemistry (ARC) approach to quickly solve reactive flow problems in the Aerospace field while preserving an acceptable accuracy of the results. The Quasi-Steady State (QSS) approximation treats the species with the smallest lifetime and concentration as steady state. The selection of the QSS species is done by means of a sensitivity coefficient, via the Level of Importance (LOI) approach, so as to include in the QSS-list the species with long lifetime but small sensitivity. An algebraic system of equations updates the concentration of the QSS species reducing the cost of ODE integration. That also helps to reduce the stiffness of the chemical ODE system, promoting an acceleration in its solution. The use of an elimination method (DAC) further accelerates the detailed-chemistry simulations. Testing is performed on two cases. Simulations are conducted via the CFD software OpenFOAM®. Two combustion models are accounted: the Eddy Dissipation Concept (EDC) and the Partially Stirred Reactor (PaSR). Solutions are validated against experimental results available in the literature.

**Key-words:** OpenFOAM, CFD, Jet in Hot Coflow, High Momentum Jet Flame, QSS Approximation, Analitically Reduced Chemistry

# Contents

# Nomenclature

| | |
|---|---|
| $\rho$ | Density |
| t | Time |
| u | Velocity |
| $\mu$ | Viscosity coefficient |
| g | Gravitational acceleration |
| $\sigma$ | Cauchy stress tensor |
| $\tau$ | Deviatoric stress tensor |
| e | Thermodynamic energy |
| K | Mechanical energy |
| q | Heat flux |
| h | Enthalpy |
| p | Pressure |
| $Y_k$ | Mass fraction of the $k_{th}$ specie |
| $j_k$ | Diffusion flux of the $k_{th}$ specie |
| $\omega_k$ | Source term of the $k_{th}$ specie |
| $q_R$ | Reaction heat |
| $c_i$ | Concentration of the $i_{th}$ specie |
| $\omega_i$ | Concentration rate of the $i_{th}$ specie |
| $r'_k$ | Reaction rate f the $k_{th}$ specie |
| $J$ | Jacobian matrix |
| $\tau^c$ | Chemical lifetime |
| $f_i$ | Relative error |
| $f_j$ | Absolute error |
| $S^S_{x,i}$ | Species sensitivity |
| T | Temperature |
| $tol_{QSS}$ | Quasi Steady State tolerance |
| X | Mole fraction |

# Introduction

In the last decades one of the most interesting problems in the Computational Fluid Dynamics (CFD) industrial community and, more in general, in the informatic area is the development of High Performance Computing (HPC) and its optimization. [1] This type of computing is composed of cluster computers which process data and perform complex calculations at high speed and in parallel. [2]
One of the main and most important project which is focused on the CFD-HPC connection is exaFOAM®.
The exaFOAM® project has the key role of studying and solving as many CFD limitations and problems as possible, especially in the exploration of massively parallel HPC architectures. The reason why the project, and so this study, focuses on HPC is that Computational Fluid Dynamics performance is remarkably worse than idealised algorithms. These performances have a worsening due to to inherent bandwidth needs, three-dimensional and time-date handling with non-sparse matrix dependencies, spatial domain decomposition requirements and I/O challenges. [3]
There is an industrial need to improve performance of software and codes and for this the purposes and the objectives of exaFOAM® project. The realization of these objectives allows the CFD transition from performances characterized by near petascale velocities to performances the order of pre-exascale.
The main objectives can be summed up as [3]:

- solve the main bottlenecks in CFD;
- realise algorithm improvements to increase HPC scalability;
- realise engineering analysis process improvements for industrial software codes such as pre-processing, post-processing and I/O;
- demonstrate performance and scalability improvements;
- achieve European leadership in different industrial areas of application (arospace, power generation, automotive, disaster prevention);
- make all the above topics accessible by European industries thanks to the development through an open-source CFD software.

In particular, the phenomenology of the combustion processes has a key role in CFD simulations because of the increasing industrial interest due to the strong connection with real world processes and phenomena. [4]
This leads to a need in the accuracy of CFD combustion simulations prediction for the study of performance and feasibility. [5] The best way to have a correct prediction of a reacting flow is to introduce the activation of the chemistry: this means that is mandatory the introduction of all of the reactions involved in the process and so the development of the kinetic mechanisms. [6]
In the majority of the cases, chemistry reactions can be constituted from hundred to thousand species, each specie characterized by his own concentration that has to be calculated with an high number of operations in each simulation timestep and for each mesh cell.
As consequence, such a simulation is directly connected to an onerous computational cost that can severely overwhelm the computational power, resulting in a high (or non-feasible) simulation time. [7] For these reason the CFD exploration in several application fields is often limited.
The proposed study is focused on the demonstration of performance and scalability improvements through the analysis of a combustion phenomenon of two different industrial cases. This analysis has been developed through two different methods: the first one with the OpenFOAM® classic chemistry solver and then with an Analytically Reduced Chemistry (ARC) approach developed together with a Quasi Steady State (QSS) species approximation. [8], [9], [10]
All the simulations presented in this work are developed by the free, open source CFD software OpenFOAM® (Open source Field Operation And Manipulation). [11], [12]
OpenFOAM® is based on C++ and it was developed first in 2004 with a large use across several engineering's sectors. The reason of his wide use both in academic and industrial fields is the huge range of applications and solvers available. In fact it is possible to use the software to study complex fluid flows with chemical reactions, solid mechanics, heat transfer, turbulence and electromagnetics. [13]
The simulation of all these mechanisms is possible thanks to the presence of a wide amount of codes, models, physic equations and libraries.
OpenFOAM® is developed independently by ESI Group that assures the quality of the released versions with numerous rigorous tests, evaluations, validations in the order of hundred per day. Tests are designed to increase code performance and scalability, trying to decrease memory usage.
Moreover in OpenFOAM® every developer has the possibility to build a new solver or to modify/increase an existing one. This allows a fast and continuous growth of the available model and guarantee a bigger and bigger community that decreases developing time of the software.

# 1. Numerical and physical models

In this section, the equations used in this work are going to be presented with a brief description. For the fluid dynamic problem, the Navier-Stokes equations regulate the evolution of the continuity and of the momentum of the flow; at the same time, the combustion problem is handled by means of chemical transport-diffusion equations plus the arising set of ODE equations which describe the change of the mass fraction and temperature over time. It will be a focus on the developed chemistry model, namely the Quasi Steady State Approximation and in the end of the chapter, it will be explained the chosen OpenFOAM® solver for this purpose with a brief introduction of the most common ones.

## 1.1. Navier-Stokes equations

In the present work physics and phenomena of reacting flows will be investigated and for this reason the Navier-Stokes (NS) equations must be introduced. The NS equations are partial differential equations which decribe the motion of viscous fluid flow. They are constituted by the mass and by the momentum balance for Newtonian incompressible fluids.
When there are compressibility effects there is a coupling between hydrodynamics and thermodynamics. The compressibility brings the need to simultaneously solve continuity, momentum and energy equations and this leads to a mandatory introduction of an energy balance equation in the NS equations.
The introduction of compressibility effects bring to the presence of the energy balance, which leads to the need of an equation of state that allows to relate pressure, temperature and density.

The solution of NS equations is complicated by the lack of an indipendent equation for the pressure, whose gradient contributes to each of the directions in space of the momentum equations.
The first equation introduced of the NS equations is the mass balance:

$$\frac{\partial \rho}{\partial t} + \nabla \cdot (\rho u) = 0 \tag{1}$$

Where the first term is the partial derivative of density over time and the second one is the divergence of the product between density and velocity.

Another component of the NS equations is the momentum balance, that is developed in the three directions of space:

$$\frac{\partial (\rho u)}{\partial t} + \nabla \cdot [\rho u \otimes u] = -\nabla p + \frac{2}{3}\mu \nabla \cdot (uI) + \nabla \cdot [\mu(\nabla u + (\nabla u)')] + \rho g + S \tag{2}$$

In the left-hand side of the Eq. (2) there are convective terms representing the inertia forces. In the right-hand side the first term represents the pressure force, the last two terms are respectively the body forces and the source term, while $\frac{2}{3}\mu \nabla \cdot (uI) + \nabla \cdot [\mu(\nabla u + (\nabla u)')]$ is the viscous term that can be obtained starting from the Cauchy stress tensor $\sigma$:

$$\sigma = -pI + \tau \tag{3}$$

where I is the 3x3 identity matrix and $\tau$ is the deviatoric stress tensor.
The assumption of the stress tensor composed by the sum of a viscous diffusion term (proportional to the velocity gradient) and of a pressure term, makes the NS equations a parabolic equation.
To reach Eq. (2) from the Cauchy stress tensor, $\tau$ is expressed as:

$$\tau = \mu(\nabla u + (\nabla u)') + \lambda(\nabla \cdot u)I \tag{4}$$

with $\lambda = -\frac{2}{3}$.
In the case of reactive flows, due to the compressibility effects, is important to clarify that is also present the energy conservation equation.
The law of energy conservation states that the total energy of an isolated system remains constant. For this reason it is valid the concept:

$$\text{Total Energy} = \text{Mechanical Power} + \text{Thermodynamic Power}$$

Due to this equation, developing the mechanical power and the thermodynamic power, the conservation of the total energy can be written as:

$$\frac{\partial(\rho e)}{\partial t} + \nabla \cdot (\rho u e) + \frac{\partial(\rho K)}{\partial t} + \nabla \cdot (\rho u K) = -\nabla \cdot q + \rho r + \nabla \cdot (\sigma \cdot u) + \rho g \cdot u \tag{5}$$

where the left hand side represents the rate of change of the total energy. The first term at the right hand side is the diffusion term, the second one is the thermal source term, the third one represents the power flux (rate of change of strain energy) and the last one is the power source where g is a body acceleration (e.g. gravity).

By decomposing the Cauchy stress tensor in its principal and deviatoric part $\sigma = \tau - pI$ and by manipulating the terms, it follows the conservation of total energy:

$$\frac{\partial(\rho e)}{\partial t} + \nabla \cdot (\rho u e) + \frac{\partial(\rho K)}{\partial t} + \nabla \cdot (\rho u K) + \nabla \cdot (up) = -\nabla \cdot q + \rho r + \nabla \cdot (\tau \cdot u) + \rho g \cdot u \tag{6}$$

With the same principle and with the substitution of the enthalpy definition which is:

$$h = e + \frac{p}{\rho} \rightarrow \rho e = \rho h - p \tag{7}$$

the energy equation can be manipulated to express the conservation of total enthalpy that takes the form:

$$\frac{\partial(\rho e)}{\partial t} + \nabla \cdot (\rho u e) + \nabla \cdot (up) = \frac{\partial(\rho h - p)}{\partial t} + \nabla \cdot [\rho u (e + p)] = \frac{\partial(\rho h)}{\partial t} - \frac{\partial p}{\partial t} + \nabla \cdot (\rho u h) \tag{8}$$

with the substitution of h as written in eq. (7) the conservation of total enthalpy takes the form:

$$\frac{\partial(\rho h)}{\partial t} + \nabla \cdot (\rho u h) + \frac{\partial(\rho K)}{\partial t} + \nabla \cdot (\rho u K) - \frac{\partial \rho}{\partial t} = -\nabla \cdot q + \rho r + \nabla \cdot (\tau \cdot u) + \rho g \cdot u \tag{9}$$

It is important to express the energy balance as function of enthalpy because in OpenFOAM® there is the possibility to use both the energy or the enthalpy equation in the solver.
In fact, in OpenFOAM® the energy equation is generally subjected to the following:

$$\frac{\partial(\rho e)}{\partial t} + \nabla \cdot (\rho u e) + \frac{\partial(\rho K)}{\partial t} + \nabla \cdot (\rho u K) + \nabla \cdot (up) = \alpha_{eff} \nabla e + \rho r \tag{10}$$

which, with respect to the complete form:

- mechanical sources $\nabla \cdot (\tau \cdot u)$ and $\rho g \cdot u$ are neglected;
- a heat flux $q = -\alpha_{eff} \nabla e$ is assumed, where $\alpha_{eff}$ is the effective thermal diffusivity and represents the sum between laminar and turbulent thermal diffusivities;
- thermal source term $\rho r$ are specific to the particular solver.

## 1.2. Convection-diffusion equations for the chemical species

For the treatment of chemistry, generic convection-diffusion equations must be introduced. The generic balance equation for mass fraction of the $k_{th}$ specie it can be written as follows:

$$\rho \frac{\partial Y_k}{\partial t} + \rho u \nabla Y_k = -\nabla \cdot j_k + \omega_k \tag{11}$$

where $j_k$ is diffusion flux of the $k_{th}$ specie and $\omega_k$ is the source term of the $k_{th}$ specie. The generic balance equation for energy of the $k_{th}$ specie is:

$$\rho \frac{\partial h_k}{\partial t} + \rho u \nabla h_k = \frac{\partial p}{\partial t} + v \cdot \nabla p - \nabla \cdot j_q + q_R \tag{12}$$

where h is the enthalpy, $j_q$ is the heat flux of the $k_{th}$ specie and $q_R$ is the reaction heat.

## 1.3. Combustion Models

When reacting flows are accounted in the simulations, there is the need to correct the value of the released heat by means of the appropriate combustion model that brings to a correct prediction of the involved phenomena. In these cases, the domain is subjected to thermo-fluid dynamic conditions that permit the development of chemical reactions involving the chemical species. This means that the choice of a proper mechanism for species mixing is required to a correct development of the simulation.
Combustion models determine the interaction between reactants and flow establishing turbulence and mixing

in the combustion chamber.
In OpenFOAM® there are several models available, the most common are reported in Tab. 1.

| Model | Description | Input | Input description |
|---|---|---|---|
| **Laminar** | Estimation of combustion as a laminar flame | | |
| **PaSR** | Divide the computational cell into two zones (reacting zone and mixing zone) | $C_{mix}$ | |
| **EDC** | Splitting field to reacting and non reacting region | Version of the model (v1981, v1996, v2005, v2016) | |
| **InfinitelyFast** | Based on the principle that mixed is burnt | C | Additional parameter C is used to distribute the heat release rate in time |

Table 1: Main OpenFOAM combustion models

A more important focus is now given to the two models used in this work: the Eddy Dissipation Concept (EDC) model [14, 15] and the Partially Stirred Reactor (PaSR) model [16].

### 1.3.1 Eddy Dissipation Concept Model

The key point in the Eddy Dissipation Concept (EDC) model is the assumption that every combustion process can occur only on the smallest spacial scales. Here the mixing between components is developed at molecular level (with the Kolmogorov characteristic length $L_k$) [17].
The EDC theory derives from the Eddy Break Up model but with a substancial difference: in the EDC model the combustion reaction occurs only if reactants are mixed at molecular level and with a sufficiently high temperature. The molecular mixing between species are determined by turbulent fluxes, called microscale phenomena. These turbulent phenomena are concentrated in isolated zones of the space that constitute a small volume with respect to the total one.
These regions are called Fine Structures (FS) with dimensions in the order of Kolmogorov scale length ($L_k$). FS are responsible of mechanic energy dissipation in internal energy and for this it can be assumed that in FS chemical species are mixed at molecular level. FS constitute in this model the reaction zone.
The key point in using the EDC model is to establish the portion of FS volume and their mass flow exchanged with the rest of the flow to predict with accuracy the chemical mixing. This model considers that the reaction occurs in the regions of the flow where the dissipation of turbulence kinetic energy takes place (FS). The mass fraction of the fine structures and the mean residence time are provided by an energy cascade model [18].
The v2005 version of the EDC model is used in this work as it is deemed as the most suited for the investigated cases, particularly after a comparison against the experimental results. It's parameters are:

$$C_\gamma = 2.1377 \tag{13}$$

$$C_\tau = 0.4083 \tag{14}$$

$$k = \frac{\gamma_L^{e_1}}{1 - \gamma_L^{e_2}} \tag{15}$$

where $e_1 = 2$, and $e_2 = 2$.

### 1.3.2 Partially Stirred Reactor Model

The second combustion model considered in this work is the Partially Stirred Reactor (PaSR) model. It is based on the assumption that a computational cell can be divided locally into two different zones: one reaction zone and one mixing zone (where reactions don't occur).
The interaction between these two zones is generated through a mass exchange because of a mixing, giving an outlet composition. This approximation can be schematized as follows [16]:

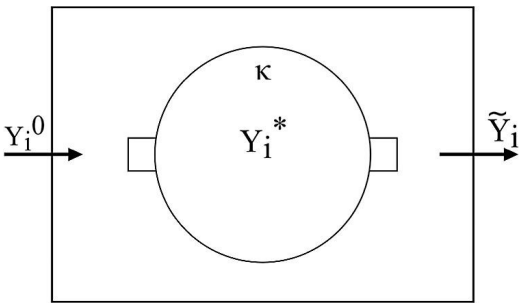


Figure 1: Computational Cell following a Partially Stirred Reactor Model (PaSR)

The figure represents a generic computational cell, where $Y_i^0$ is the initial $i_{th}$ species mass fraction in the zone without chemical reactions, $Y_i^r$ is the $i_{th}$ species mass fraction in the reaction zone and $Y_i$ is the $i_{th}$ final species mass fraction of the cell.
An important parameter in this model (and in OpenFOAM®) is the mass fraction of the reaction zone ($k$). Thanks to the determination of k, the formation rate $\dot{\omega}$ is defined.
From an informatic point of view, the OpenFOAM® algorithm expresses k with an *if* cycle that takes into account the characteristic times of the phenomenon.
These times are: the characteristic chemical time $\tau_c$ and the mixing time $\tau_k$. The principles that regulate the algorithm to determine these parameters of the model are:

- calculation of $\tau_k$:

$$\tau_k(i) = C_{mix}\sqrt{\max\left(\frac{\mu_{eff(i)}}{\rho(i)(\epsilon(i)+\xi)}, 0\right)} \tag{16}$$

  where: $C_{mix}$ is the input parameter, the mixing coefficient and it is 1 for laminar flows, 0 for extremely turbulent flows, between 0.001 and 0.3 for typical turbulent flows; $\mu_{eff}$ is the dynamic viscosity; $\rho$ is the density; $\epsilon$ is the turbulence kinetic energy dissipation; $\xi$ is equal to 1e-6.
- *if* cycle that determines k value:
  - *if* $\tau_k > \xi$

$$k = \frac{\tau_c}{\tau_c + \tau_k} \tag{17}$$

  - *if* $\tau_k < \xi$

$$k = 1 \tag{18}$$

- the return of k · R(Y) and of k · $Q_{dot}$. R(Y) is the fuel consumption rate and $Q_{dot}$ is the heat release rate.

So, k defines the formation rate of a certain species: when the mixing time $\tau_k$ is smaller than the chemical one $\tau_c$, k = 1 and mixing is efficient with the result that the final composition is determined by chemistry; if the opposite happens, k = 0 and the final composition is given by the mixing.
The formation rate is equal to:

$$\dot{\omega}_i = k\frac{\rho(Y_i^r - Y_i^0)}{\tau_k} \tag{19}$$

## 1.4. Chemistry Models

Since combustion involves multiple species reacting through an elevate number of chemical reactions. The number of chemical reactions can rapidly increase and include a high number of reacting species. This leads to several additional terms in Navier-Stokes equations. Chemical species in reactive flows are characterized by reaction rates that require specific modeling (to deal with mixtures, transport coefficients such as heat diffusivity, species diffusion, viscosity, etc.).
The presence of chemical reacting substances brings to the development of chemical combustion products when the energetic level of the "activation energy" is reached. In OpenFOAM simulations the chemical reactions are phenomena that require a special attention due to their own nature:

- chemical reactions are usually strong exothermic or endothermic phenomena; this means that are characterized by steep temperature and energy gradients;
- they are extremely fast phenomena with the consequence that they have to be treated with a smaller timestep with respect to fluid dynamics phenomena. Otherwise some important results can be wrong processed;

- since there is the presence of mixture of gases, it must be treat with specific attention the tuning of transport coefficients (heat diffusivity, species diffusion, viscosity, etc.).

A typical chemical reaction is structured as follows (thanks to the Penner's formalism):

$$A \Longleftrightarrow B \tag{20}$$

$$A + B \Longleftrightarrow X + Z \tag{21}$$

$$\sum_{i=0}^{n} \nu_i' M_i \Longleftrightarrow \sum_{i=0}^{n} \nu_i'' M_i \tag{22}$$

where:

- $\nu_i'$ is the $i_{th}$ stoichometric coefficent for reactants;
- $\nu_i''$ is the $i_{th}$ stoichometric coefficent for products;
- $M_i$ is the $i_{th}$ chemical species of mixture;
- n is the total number of species in reactions

In these simulations a chemistry activation process leads to solve a system of Ordinary Differential Equations (ODEs). This system depends on the number of the involved species and on the number of reactions. The chemical process produces a variation of the chemical species concentrations.

By means of the treatment of the chemical problem via the solution of a system of ODEs, the computational cost of the simulation is high. The reasons are: the introduction of an high number of equations that must be solved, OpenFOAM code nature which create a cycle on the cells that have to be solved one after the other.

Chemistry activation is linked to time and it depends on the mesh resolution: because of the high number of species and reactions each cell, together with an elevated number of cells means a need to solve an elevated number of equations overall. In the OpenFOAM® software the timestep is controlled by the ODEs solution stability, by the chosen integration scheme and by the chemical phenomenology. The chemistry timestep is much smaller than the fluid dynamics one.

### 1.4.1 Quasi Steady State Approximation

In a reactive configuration, the chemical kinetics mechanisms can be described by a ordinary differential equations system that can be expressed as:

$$\frac{\partial c_i}{\partial t} = \omega_i \tag{23}$$

where $c_i$ is the $i^{th}$ specie concentration and $\omega_i$ can be expressed as:

$$\omega_i = \sum_{k=1}^{N_r} r_k' \cdot (v_{i,k}'' - v_{i,k}') \tag{24}$$

In the last equation $r_k'$ is the raction rate, $v_{i,k}''$ and $v_{i,k}'$ are the stoichiometric coefficients of the $i^{th}$ specie in the $k^{th}$ reaction, of the products and of the reactants respectively.

The guiding principal of the Quasi-Steady-State approximation (QSSA) is the replacement of several ordinary differential equations by algebraic ones. The main assumption of QSSA is that some of the chemical processes occur on timescales much smaller than the physical ones. Once one of the species is approximated as Quasi Steady, the source term is assumed to be zero. Thanks to this assumption it is valid to assign the right hand side of eq. (23) to zero.

With this method the concentration vector can be divided into two groups: $C = (C_1, C_2)$ where $C_1$ are linked to the non-QSS species and $C_2$ are linked to the QSS species. Eq. (23) can be written thanks to a formulation which has the presence of the Jacobian matrix as follows:

$$J = \begin{pmatrix} J_{11} & J_{12} \\ J_{21} & J_{22} \end{pmatrix} = \begin{pmatrix} \frac{\partial \omega_1}{\partial c_1} & \frac{\partial \omega_1}{\partial c_2} \\ \\ \frac{\partial \omega_2}{\partial c_1} & \frac{\partial \omega_2}{\partial c_2} \end{pmatrix} \tag{25}$$

Thanks to the QSS approximation the system becomes:

$$\frac{dC_1}{dt} = \omega_1 \tag{26}$$

$$\frac{dC_2}{dt} = 0 = \omega_2 \tag{27}$$

In this way it is created a set of algebraic equations describing the species conservation. The set generated with this approximation can present quadratic terms due to the presence of multiple QSS species in some elementary reactions in the kinetic chain. For this reason the system isn't necessarily linear.
The entire problem becomes an eigenvalue problem characterized by fast and slow modes. Fast modes can be neglected and they are represented by the species treated as Steady State. The decisional procedure of the algorithm which establish how to detect a QSS specie is based on the chemical lifetime that it is represented by diagonal terms of the Jacobian matrix of eq. (25). In fact with the assumption of a diagonal Jacobian matrix, the chemical lifetime can be expressed as [19]:

$$\tau_i^c = -1/J_{ii} \tag{28}$$

Expliciting the jacobian diagonal terms, eq. (28) becomes:

$$\tau_i^c = -\frac{1}{\frac{\partial \omega_i}{\partial c_i}} = \frac{c_i}{\sum_{k=1}^{N_r}(v''_{i,k} - v'_{i,k})v'_{i,k}r'_k} \tag{29}$$

A mathematical justification of the Eq. (28) is presented in appendix A [20].

The jacobian computation usually has an onerous computational cost. For this reason, its calculation is designed to occur only after the mechanism has been reduced. In this way, the computational cost to perform such an operation severely diminishes. In fact, after the reduction, only the active species have to be accounted, thus shrinking the dimensions of the jacobian matrix, and the cost of finding its inverse. Moreover, to consider only diagonal terms such as species chemical life means not to consider any type of coupling between species. This is a good approximation for species with small timescales beacuse a large $J_{ii}$ indicates a fast decay of perturbations and for this reason the errors can be tolerated. This approximation indicates that the species with small lifetime can be set as QSS without the introduction of a significant error.

One of the key aspects of the application of the QSS approximation reduction method is that there is an introduction of an error into the system. When a steady-state species concentration is approximated, its absolute error can be expressed as:

$$f_j = \frac{\partial c_j}{\partial c_i} f_i + \sigma(f_i^2) \tag{30}$$

where the first RHS factor represents the sensitivity of species j towards species i.
In the case of QSSA, with the application of chemical lifetime $\tau_i^c$ as a selection parameter for the steady-state species, the chemical lifetime is proportional to the relative error $f_i$. This is the reason why the following proportionality has been investigated in [21]

$$\frac{f_i}{c_i} = \tau_i^c \rightarrow f_i \propto c_i \tau_i^c \tag{31}$$

Eq. (31) is valid until a certain value of $\tau_i^c$ where non-linear effects become predominant.
As shown in [21] the tendency is clearly that the errors introduced by the QSSA increase with a monotonic trend with lifetime. However, the error introduced by a certain specie is not always dependent only on lifetime: some species have a short life but have to be kept into the mechanism to avoid the introduction of a large error; on the other hand, some longlife species are considered as Steady State because of their nature (i.e. exhausted gas emission or flame speed). That avoids the introduction of a large error.
This brings to the fact that a choice of QSS species based only on the chemical lifetime cannot be an accurate solution and it can lead to completely wrong results. The key point is to find a method that while avoiding the introduction of relevant errors it eliminates: a) all the species with small lifetime; b) all the species with a long lifetime whose effect on the chemical evolution of the reaction is anyway limited. All these species can be treated as QSS. In this way QSSA creates a reduced reaction mechanism that allow to develop CFD simulations with a smaller computational cost while maintaining at the same time an high level of accuracy.
For the reasons cited above, one possible way to utilize the QSSA approach is to develop a sensitivity study. Several methods to automatically identify suitable QSS species based on their sensitivity can be found in literature [22–25]. One of the most interesting criterion for this type of study has been treated in [21, 26] where a parameter called Level of Importance (LOI) has been introduced. In the cited study, an estimation of instantaneous error of the steady state species concentration has been developed.
With this LOI approach, a sensitivity coefficient is introduced so that all the species with long lifetime but small sensitivity can be treated as QSS. A generic definition of LOI coefficient can be:

$$LOI_i = S^S_{x,i} c_i \tau_i \tag{32}$$

with $S^S_{x,i}$ representing the species sensitivity of a relevant parameter x on species i.
This parameter can introduce an error that can be expressed as the chemical lifetime error:

$$f_x = \frac{\partial x}{\partial c_i} f_i + \sigma(f_i^2) \tag{33}$$

As before the first term in the RHS is composed by the species sensitivity of the chosen parameter on species i, $S^S_{x,i}$, and $f_i$ that is proportional to the chemical lifetime.

In the QSS approximation a key aspect is the tuning of the tolerance. At the beginning of the simulation the tolerance assumes the same value of the chemical timestep but it has to be changed because when the temperature has steep gradient, the tolerance has to be lower. In the analyzed cases a phenomenon that presents steep gradients is the ignition: it is a fast event and for this QSS species has a smaller lifetime than the one of a physical event (such as the mixing). In the same way, when it is present a gradual gradient more species can be approximated as QSS. The tolerance must assume the same behavior of the timestep and it must vary during the simulation. For this reason, in this work, the value of the tolerance changes every timestep following the temperature evolution and the local step.
In order to develop this approach, the tolerance has been related to the slope of the temperature that expresses the evolution of the temperature in time. This is defined as:

$$T_{slope} = \text{mag}\left(\text{atan}\left(\frac{dT}{dt}\right)\frac{180}{\pi}\right) \tag{34}$$

At this point, the tolerance is defined as:

$$tol_{QSS} = maxTol_{QSS} + (minTol_{QSS} - maxTol_{QSS})\frac{T_{slope}}{90}\frac{(1+q)}{\frac{T_{slope}}{(90+q)}} \tag{35}$$

with q = 0.01. In eq.(35) $maxTol_{QSS}$ and $minTol_{QSS}$ have been introduced. These two parameters are user inputs and some tests showed that higher values of the two parameters determine a consideration of more QSS species but a reduction of reliability bringing to incorrect results. Moreover the values of the two tolerances are case dependent and a correct initial tuning has a fundamental role in the simulation development.
Fig. (2) shows the variation of the tolerance on the angle of the temperature gradient in function of the q. As it can be seen, higher is the value of the q and more gradual will be the variation of the QSS tolerance.

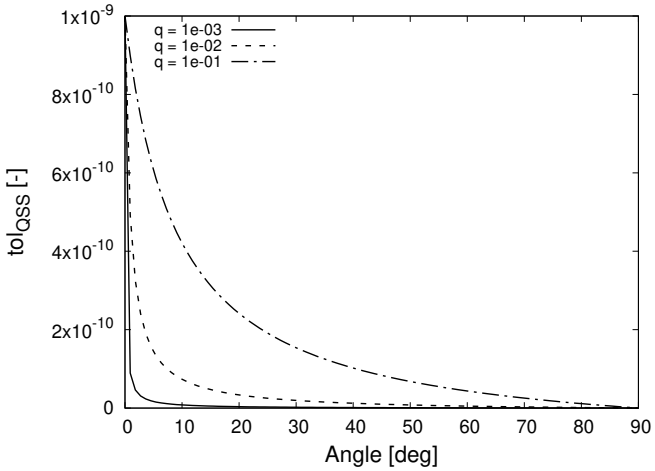


Figure 2: Influence of the q function on the $tol_{QSS}$

## 1.5. OpenFOAM® Solvers

For the validation, OpenFOAM® has been used, exploiting a solver which allows the treatment of reacting flows simulations.
Multiple solvers are available in OpenFOAM to handle these kind of scenarios. Due to the nature of the problem,

the flow is characterized by different type of phenomena. In fact, phenomena with different nature are involved, such as compressibility, combustion and chemistry.
Some of the main solvers that OpenFOAM provides for these types of applications are:

- chemFoam;
- coldEngineFoam;
- engineFoam;
- fireFoam;
- reactingFoam;
- XiFoam;

In the present work, transient, compressible and reactive flows cases have been analyzed. Moreover there is a particular interest in the detailed chemistry of the problem. Due to the presence of multiple transported species and the multicell nature of the simulations, reactingFoam is the only solver that respects all the involved requirements because is the only solver that simulate these type of flows in a multicell environment.
Due to these features reactingFoam is used as solver for multicell combustion with chemical reactions.
To solve these type of systems, reactingFOAM uses stoichiometry expressions, in this way, the substances that are involved in the reactions, completely react. The usage of reactingFoam allows to obtain the development of species rate consumption and production that, together with a correct thermophysical model, is capable to predict the correct fluid mixture phase.

The reactingFoam solver is based on the rhoPIMPLE algorithm, which derives from the PIMPLE one.
PIMPLE is a combination of PISO (Pressure Implicit with Splitting of Operator) and SIMPLE (Semi-Implicit Method for Pressure-Linked Equations).
the PIMPLE algorithm (as the PISO one) is used for transient cases. On the contrary, SIMPLE is used for steady-state cases. A scheme of the PIMPLE algorithm is reported in fig. 3a:

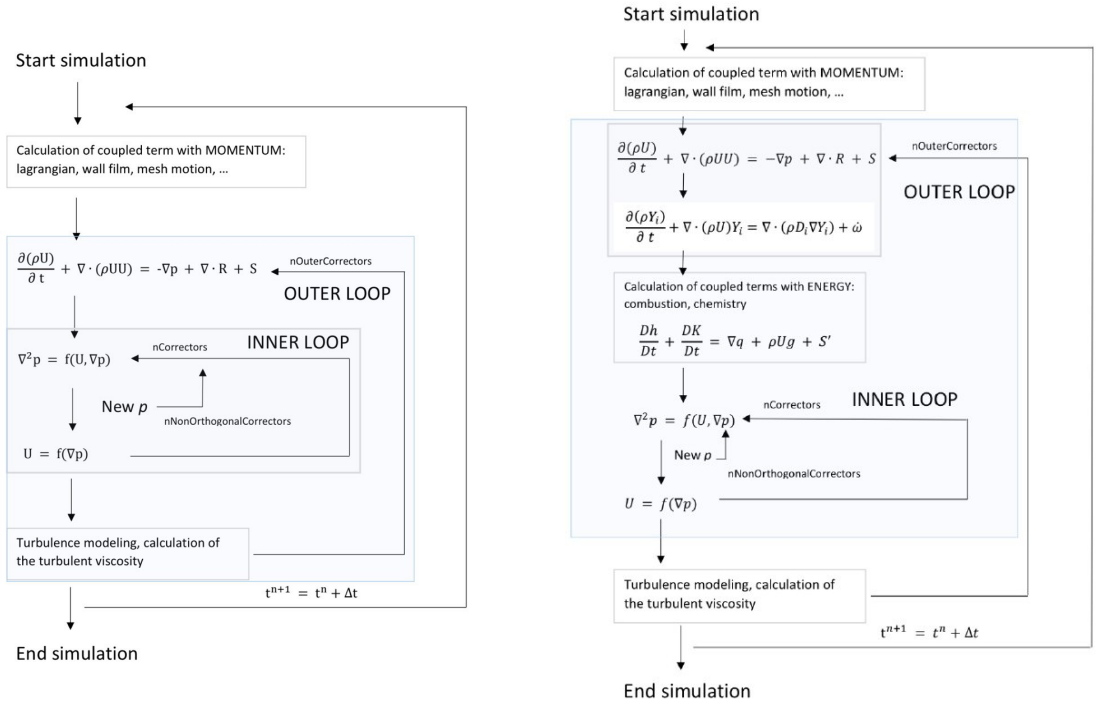


(a) Pimple Algorithm (b) ReactingFoam Algorithm

Figure 3: OpenFOAM Algorithms

Fig. 3 shows a comparison between the PIMPLE algorithm and the rhoPIMPLE algorithm. The main difference between the two is the presence of all the terms that are coupled with energy. For this reason the loop is augmented and this allows to solve the energy equation (see Eq. (5)) and the equations of transport-diffusion of the chemical species (see Eq. (12)).
A generic form of the equation, which calculates the coupled terms with energy, can be expressed as follows:

$$\frac{Dh}{Dt} + \frac{DK}{Dt} = \nabla q + \rho U g + S' \tag{36}$$

## 2. Auto-ignition of a methane jet in a Hot Coflow

The first analyzed case is the auto-ignition of a turbulent methane jet in a hot vitiated coflow. A fuel jet is introduced in a region of air that has already undergone a combustion process; the mixture is ignited and generates a steady lift flame.
The experimental data is compared with the numerical simulation using the reactingFoam solver from OpenFOAM®. In this simulation, two geometries have been used, namely:

- a 3D, constituted by a quarter of the combustion chamber (representation that is possible thanks to the symmetry of the chamber). This geometry requires an higher computational time. The aim of the 3D case is to develop a tutorial case for academic use that allows: a) to have a double check of the accuracy of the wedge case; b) to study the problem with a different point of view; c) the validation through the same methods of the wedge case.
- a wedge, developed to obtain results with a lower computational time and cost. The aim of the wedge case is to develop a tutorial case that allows the validation through: a) the methods that are already implemented in OpenFOAM®; b) the QSSA proposed in this study. The results of the simulations are compared against experimental results available in the literature. This test serves for academic use.

For a correct comparison between experimental and numerical data, the experimental set-up is taken from [27].

### 2.1. Experimental set-up

The experiment is conducted by the DLR (Deutsches Zentrum für Luft und Raumfahrt) Institute of Combustion Technology [27]. The geometry of the burner used in the experiment is shown in Fig. 4:

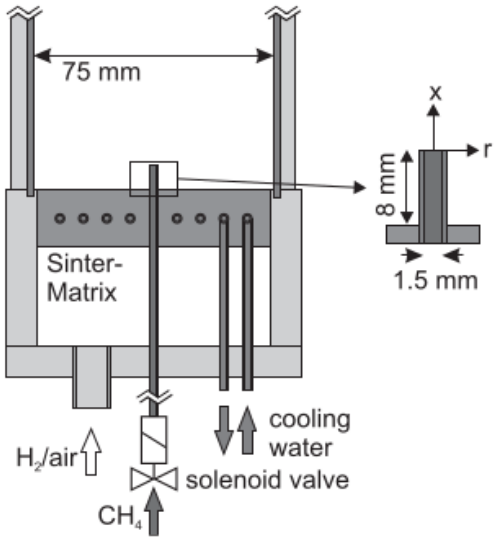


Figure 4: JHC Burner [27]

The nozzle has a 1.5 mm diameter, is placed in the center of the combustion chamber. The squared area of the chamber measures 75x75 $mm^2$ and at its bottom a matrix burner is present in order to stabilise the exhaust gases.
The composition of burnt gases is given by [28] and is reported in the tab. 2:

| **Species** | $O_2$ | $H_2O$ | $N_2$ | OH |
|---|---|---|---|---|
| **X** | 0.1021 | 0.1782 | 0.7196 | 0.00163 |

Table 2: Composition of coflow expressed in mole fraction (X)

The coflow enters the chamber with a velocity U = 4.1 m/s, a temperature T = 1490 K and an ambient atmospheric pressure.

Different conditions are accounted for the methane jet: it is introduced in the chamber with a mass flow $\dot{m}$ = 0.2067 g/s and a temperature T = 290 K.

## 2.2. 3D geometry setup

As previously stated, a 3D geometry is considered in this first sub-test: the combustion chamber has a square base (75mmx75mm) with a central fuel inlet. The height differs from the two base dimensions and it is equal to 120mm.
For the proposed simplification, because of the double-symmetry experienced along the height of the chamber, only a quarter of the domain is investigated. In face of this reduction of the domain, two sides of the resulting geometry are set as symmetrical planes (see darker layers in fig. (5b. The small centered nozzle, that can be seen in fig. (4), injects the fuel, while air with lean premixed hydrogen combustion products is introduced at the bottom of the mesh in the surrounding region. Since at the center of the burner is present a single round injector, the introduced symmetries allow the investigation of a quarter of the entire geometry.
The mesh is created with the blockMesh application and the file receives as input the average mesh size to set an appropriate number of cells with the possibility of different levels of refinement. when no inputs are provided, default average mesh size and values of refinements are set. The number of cells in the y direction is automatically adjusted to preserve the cells aspect ratio according to the selected refinement.
Details of the geometry are present in Fig. (5) and (6):

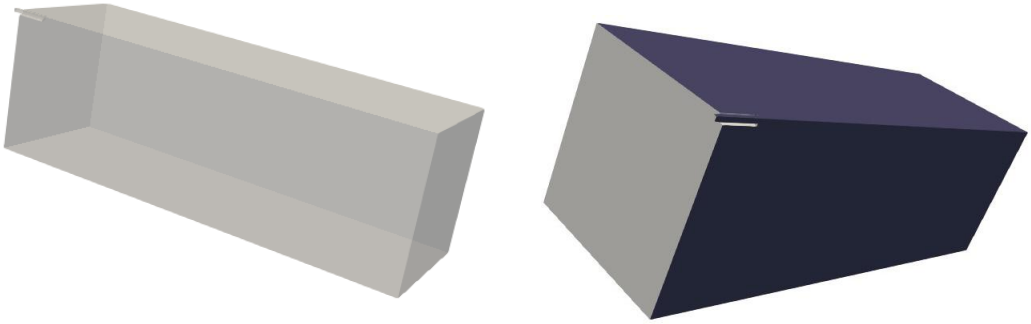

(a) View of the chamber (b) Symmetry planes of the chamber

Figure 5: 3D Mesh

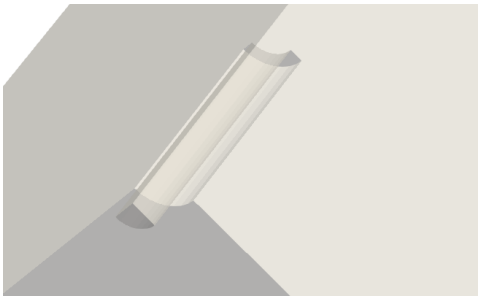

(a) Fuel inlet region

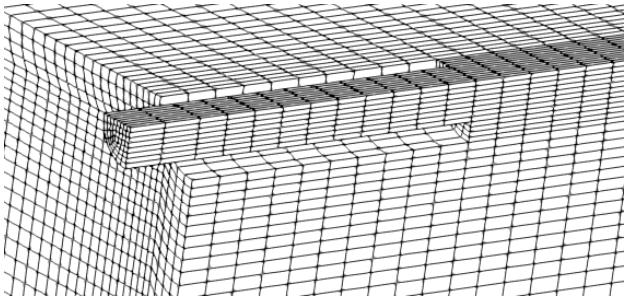

(b) Fuel inlet discretization

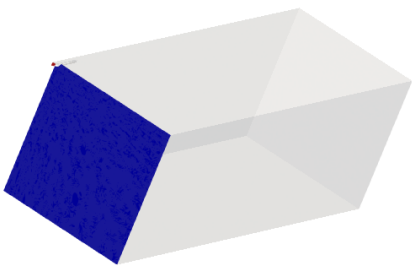

(c) Air inlet in blue, methane inlet in red

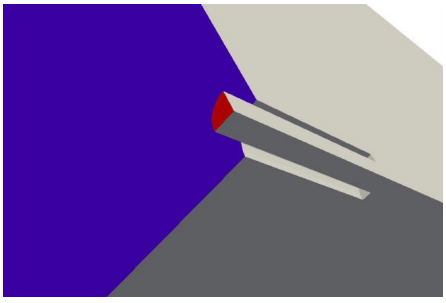

(d) inlets in detail

Figure 6: 3D Mesh: inlet details

The case is three-dimensional and simplifications are introduced to reduce domain complexity and consequently to reduce both computational cost and time. The boundary and the initial conditions are set accordingly.
In the tab. (3) are presented the initial and boundary conditions of the treated case:

| **Region** | Field | Description | Type | Value |
|---|---|---|---|---|
| **Internal field** | p | Pressure | uniform | 1e5 Pa |
| | T | Temperature | uniform | 600 K |
| | $\epsilon$ | Turbulent mixing length dissipation rate | uniform | 2 |
| | U | Velocity | uniform | 4.1 m/s |
| **Fuel inlet** | U | Velocity | fixedValue | 2.067e-4 g/s |
| | T | Temperature | fixedValue | 600 K |
| | $\rho$ | Density | | 0.71682 kg/$m^3$ |
| | k | Turbulent kinetic energy | uniform | 0.375 |
| | $\epsilon$ | Turbulent mixing length dissipation rate | uniform | 0.005 |
| | $Y_{CH_4}$ | Methane mass fraction | fixedValue | 1 |
| **Air inlet** | U | Velocity | fixedValue | 4.1 m/s |
| | T | Temperature | fixedValue | 1490 K |
| | k | Turbulent kinetic energy | uniform | 0.02 |
| | $\epsilon$ | Turbulent mixing length dissipation rate | uniform | 0.005 |
| | $Y_{O_2}$ | Oxygen mass fraction | fixedValue | 0.1021 |
| | $Y_{N_2}$ | Nitrogen mass fraction | fixedValue | 0.71807 |
| | $Y_{OH}$ | Hydroxide mass fraction | fixedValue | 0.00163 |
| | $Y_{H_2O}$ | Water mass fraction | fixedValue | 0.1782 |

Table 3: Initial and boundary conditions for the 3D geometry case

Moreover the quantities connected to sides are set to symmetry thanks to the simplification introduced by the symmetry planes definition.
At the walls, a no-slip boundary condition is applied for U, while a zero gradient condition is applied for p and T; wall functions are set according to compressible k-$\epsilon$ model for turbulence-related quantities.

## 2.3. Wedge setup

As previously stated, a wedge geometry is considered in this second sub-test: the shape is developed as a clove of 2° of the total chamber with a blockMeshDict. This introduces a first approximation to the problem because the 360° projection of the clove generates a cylindrical chamber instead of a square one. This approximation is deemed acceptable as the near-wall effects can be neglected due to their marginal contribution to the overall evolution of the combustion.
Details of the geometry are reported below:

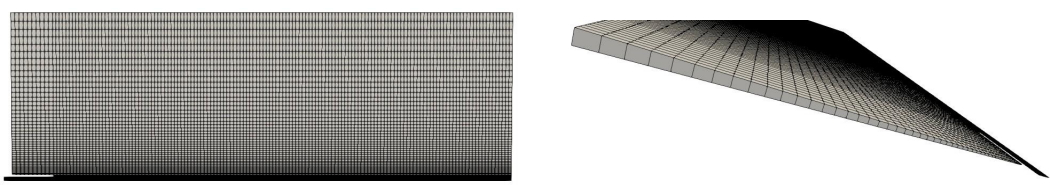

(a) zy plane view (b) Transversal view

Figure 7: Wedge Mesh

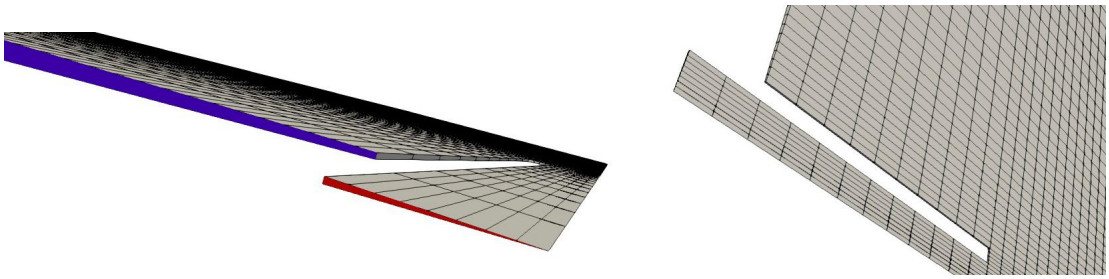

(a) Air inlet in blue and methane inlet in red (b) inlet patches discretization

Figure 8: Wedge Mesh: inlet details

This type of geometry represents a tutorial case that allows to have a small computational time with a smaller memory usage.

The initial and boundary conditions of the wedge case are presented in Tab. (3) beacuse are setted equal to the one of the 3D geometry.

## 2.4. Numerical setup

In this section, a description is presented of all the choices that have been implemented numerically to obtain a sufficiently accurate comparison against the experimental case.
Regarding the combustion model adopted in the simulation, it has been used the Partially Stirred Reactor (PaSR) model, introduced in section 1.3.2. The characteristic coefficient is equal to $C_{mix} = 1$.
The presence of turbulence in the treated phenomenon leads to choose a turbulence model. A $k - \epsilon$ model has been selected for this set of simulations because this model is more suitable with respect to the k - $\omega$ model. $k - \epsilon$ model, based on the standard model [29] and on the rapid distorsion theory compression term [30], is developed trough two transport equations, each of which is dependent on a specific unknown, namely: the turbulent kinetic energy k and the turbulent kinetic dissipation $\epsilon$.
Regarding the chemistry two different approaches have been used: the ODE solver already implemented in OpenFOAM® and the QSSA developed model. In both cases an implicit ODE solver, the Seulex one, has been tested.
In these auto-ignition cases, numerical schemes for involved terms have been set in the fvSchemes dictionary in the system directory. The localEuler (first order) scheme has been selected to handle time derivatives, it is a pseudo transient scheme, set by specific Local Time Stepping (LTS) solvers. A second order Gauss integration scheme is instead used for the gradient terms, as well as for the Laplacian scheme. In particular, for the latter, a Gauss linear orthogonal scheme is picked.
In the dictionary that set the schemes required for the handling of divergence operations a second order, unbounded, Gauss limitedLinear scheme has been selected for all terms. The reactingFoam application solver has been used in the simulation, as anticipated in section 1.5. The simulation has been set for both the built geometries to end at 10000 timesteps with a maximum Courant number equal to 0.2.

## 2.5. Results

### 2.5.1 Comparison between wedge and 3D geometry

In the auto-ignition of a methane jet in a hot coflow case, two simulations has been run. In fact, the wedge geometry case and the 3D geometry one, have been run with the same setup, to have a comparison between the two and to show that both of the geometries generate a satisfied agreement in the results.
In Fig. (9) it has been compared the temperature at the final step of the simulation inside the whole domain. In the comparison it can be seen that the temperature scales are, for both the simulations, between 600 K and 1900 K and there is an identical behavior of the temperature contour lines that are developed with a very similar trend.
It is important to underline that in the two figures the geometries seems to be different: this is because to make a correct comparison for the 3D geometry it has been considered a 45° slice in the domain. This generates a length of 0.0566 (0.04/sin(45°)). The difference between the two length does not represent a problem for the comparison because effects near the external wall are not significant.

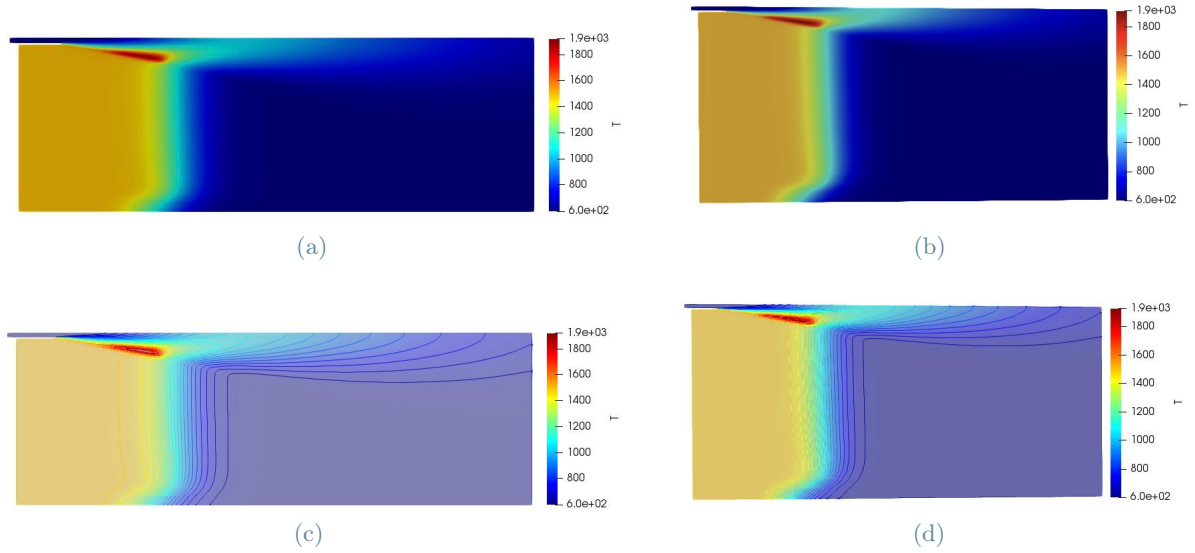


(a) (b)

(c) (d)

Figure 9: Temperature comparison: (a) and (c) refer to wedge geometry, (b) and (d) refer to 3D geometry)

In Fig. (10) it is shown the temperature curve of the two simulations along several axial lines. Four different axial lines have been set at a distance on the z axis equal to 15mm, 20mm, 25mm and 30mm. For the axial lines position, the region where reactions occur was chosen.
In every graph, the behavior of the temperature is the same with some small difference: in the 3D geometry, the increment of temperature occurs nearest to the fuel inlet with a maximum difference of 50 K (2.5% deviation) in the 25mm axial line. This behavior is justifiable by the nature of the geometries: in the wedge the distance between the reactions and the walls is different with the respect to the 3D one.

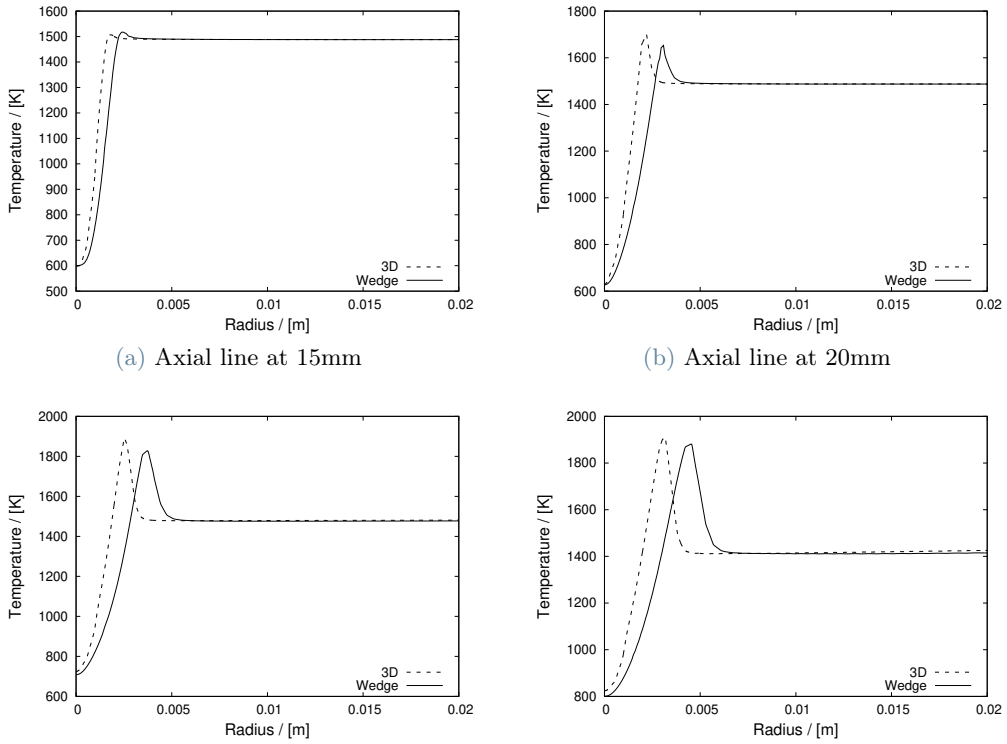


(a) Axial line at 15mm (b) Axial line at 20mm

(c) Axial line at 25mm (d) Axial line at 30mm

Figure 10: Temperature comparison between wedge and 3D geometry with different axial lines

Another interesting comparison developed between wedge and 3D is presented in Fig. (12). The figure shows

sixteen different graphs where every graph contains the comparison of the temperature evolution in time between the two geometries. Each graph represents a single point taken inside the mesh. The chosen region is shown in Fig. (11) and it corresponds to the region where the combustion and the flame front are developed.
The comparison shows a similar behavior of the two geometries with a little variation in the points where the temperature reach the higher values, correspondent to the evolution of the combustion.

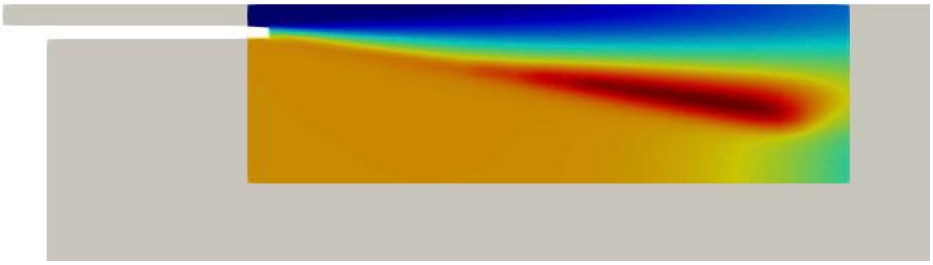

Figure 11: Probes region

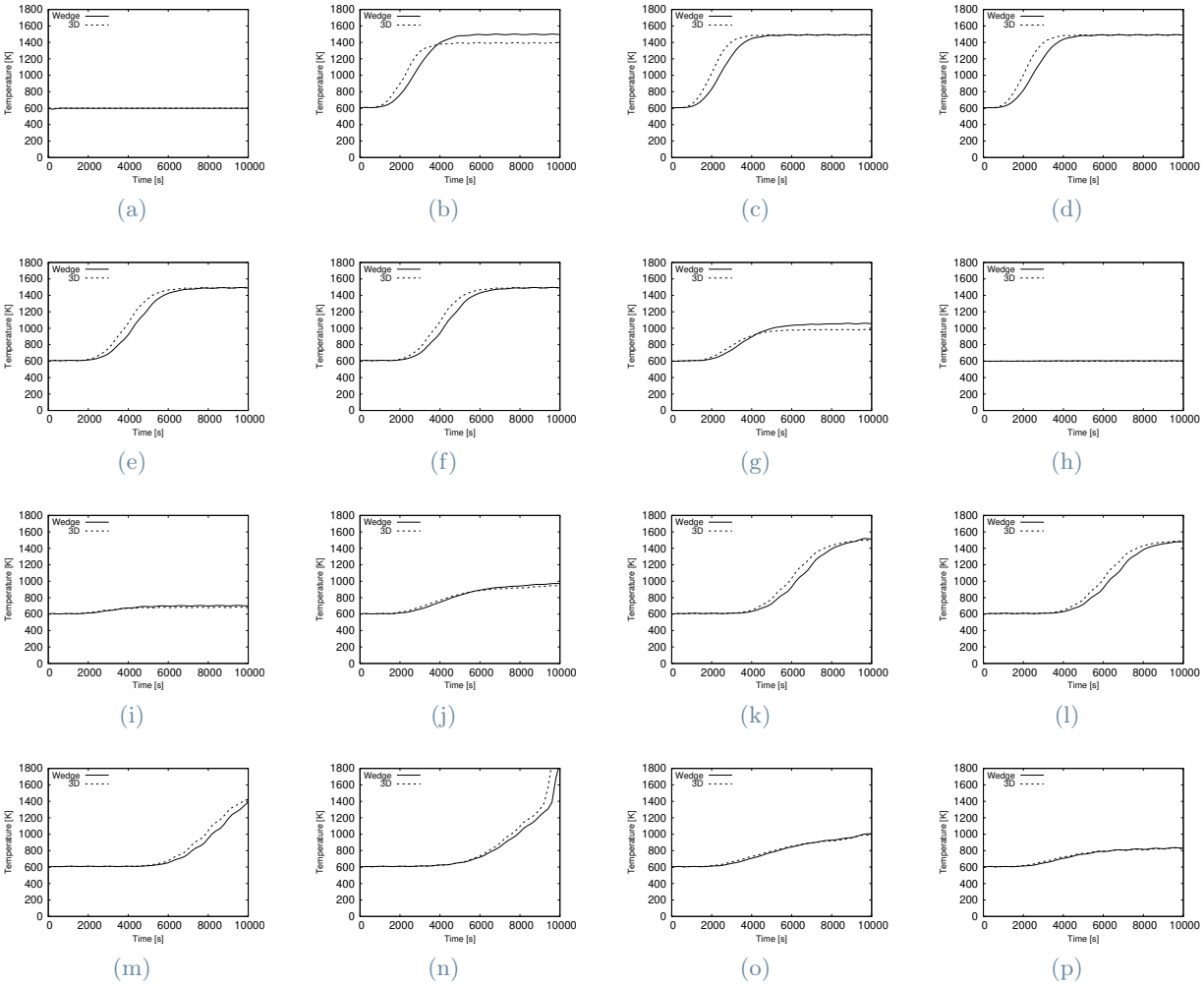


Figure 12: Comparison of temperature over time between wedge and 3D geometry in 16 points of the domain

In Fig. (13, 14) a deeper comparison has been developed. The velocity and the $CO_2$ behaviors are shown, underlying, such as the temperature, a similar developing.

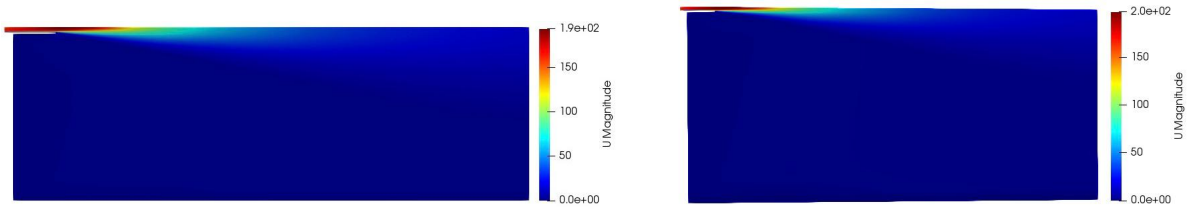


(a) Wedge geometry (b) 3D geometry

Figure 13: Velocity comparison

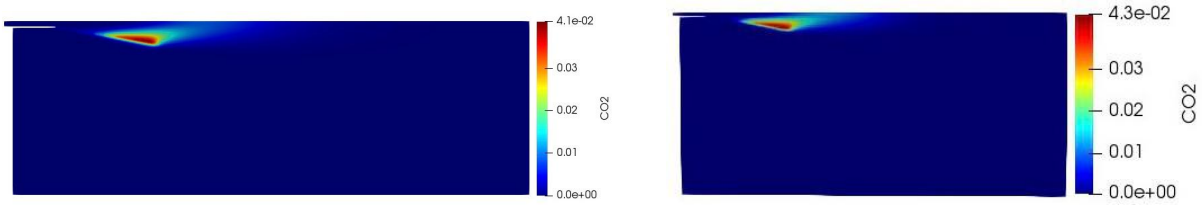


(a) Wedge geometry (b) 3D geometry

Figure 14: CO2 comparison

### 2.5.2 Comparison between the wedge geometry simulation and experimental results

Thanks to the comparison between the two described geometries and the results obtained in the section (2.5.1), the experimental results have been compared to the wedge numerical results. This allowed to save computational cost and time keeping an high precision and reliability. Fig. (15) presents the obtained results.

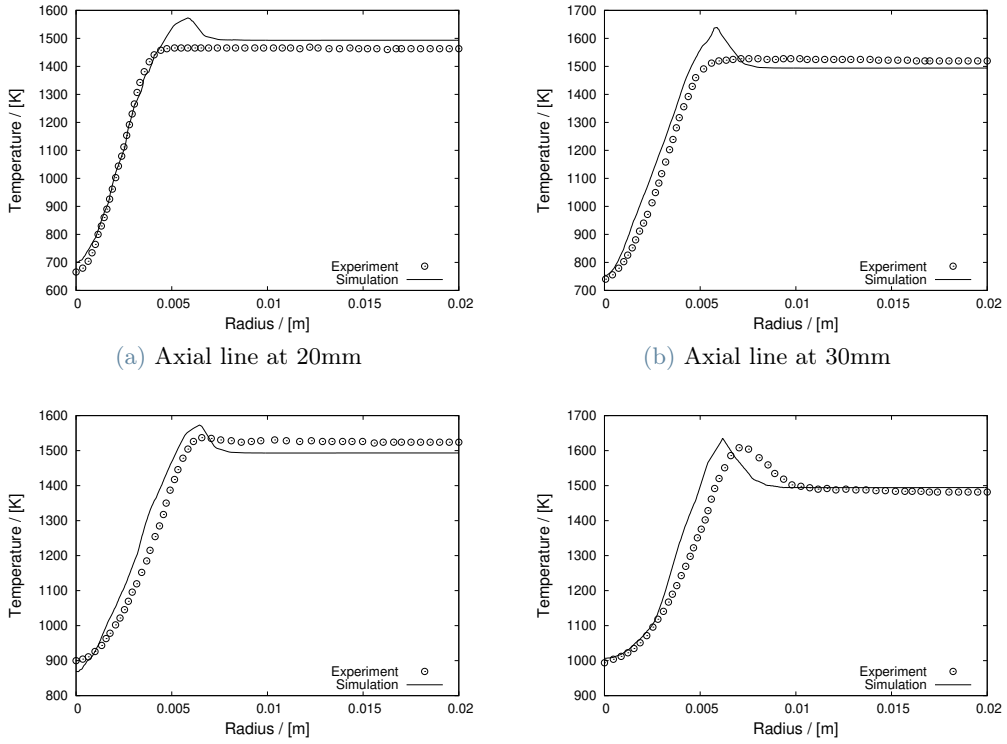


(a) Axial line at 20mm (b) Axial line at 30mm

(c) Axial line at 40mm (d) Axial line at 50mm

Figure 15: Temperature comparison: simulation vs experiment

Fig.(15) shows a comparison of the temperature on different axial lines arranged along the length (z axis) of the chamber. In every graph, the trend of the simulation has almost the same trend of the experimental data. The

difference between numerical and experimental results can be noticed in a small overshoot in the corresponding part of the front flame. The overshoot has a maximum difference in the nearest axial line (fig.(15a)) with respect to the fuel inlet and it is equal to 80 K (5% difference). This denotes that the front flame is developed nearest the fuel inlet with respect to the experimental case. In the fig.(26a) there is the minimum difference between the two cases, difference of about 40 K (equal to 2%).
The presence of the overshoot can be explained with wall effects: with the wedge geometry development a wall region has been set near the fuel inlet, this can create a critical region where turbulence is present causing an increment of temperature and generating the overshoot. Another reason to this temperature difference can be caused by the combustion model and the chemistry mechanisms setting. In the simulation it has been used the PaSR model for the combustion, with a $C_{mix}$ coefficient equal to 1, and it has been used the GRI mechanism for the chemical evolution. These choices can lead to the described difference and a deeper study with a different tuning could lead to better results.

### 2.5.3 Comparison between classical approach and ARC approach in wedge geometry

Thanks to the comparison of section 2.5.1, it was possible to run, with the ARC method option, only the wedge geometry case, with an high computational cost and time saving.
As anticipated, the comparison between the 'classic' resolution of the ODEs system and the QSS approximation has been developed. The validation has been performed comparing the temperature profile of both cases and focusing on the execution time of the two simulations. In the development of the QSS approximation tuning, a trade-off between time and accuracy must be found and this has been done with a meaningful choice of the two tolerances: maxTolQSS equal to 1e-6 and minTolQSS equal to 1e-7.
The same temperature comparison of section 2.5.1 has been developed in Fig. (16) where the two temperature profiles reflect the same trend at each axial line considered. In this comparison four different axial lines have been considered, respectively at 15mm, 20mm, 25mm and 30mm on the length of the chamber (z axis).
The comparison shows a difference between the ARC and classical approach in the flame front region with a maximum discrepancy in the peak of the 30mm axial line, the farest from the fuel inlet. In this point the difference is equal to 120 K (5.5% of the maximum temperature).
These results demonstrate that the ARC approach does not take completely the behavior of the combustion phenomenon and the development of the chemistry reactions. In fact, there is an under estimation of the peak temperature of the combustion.

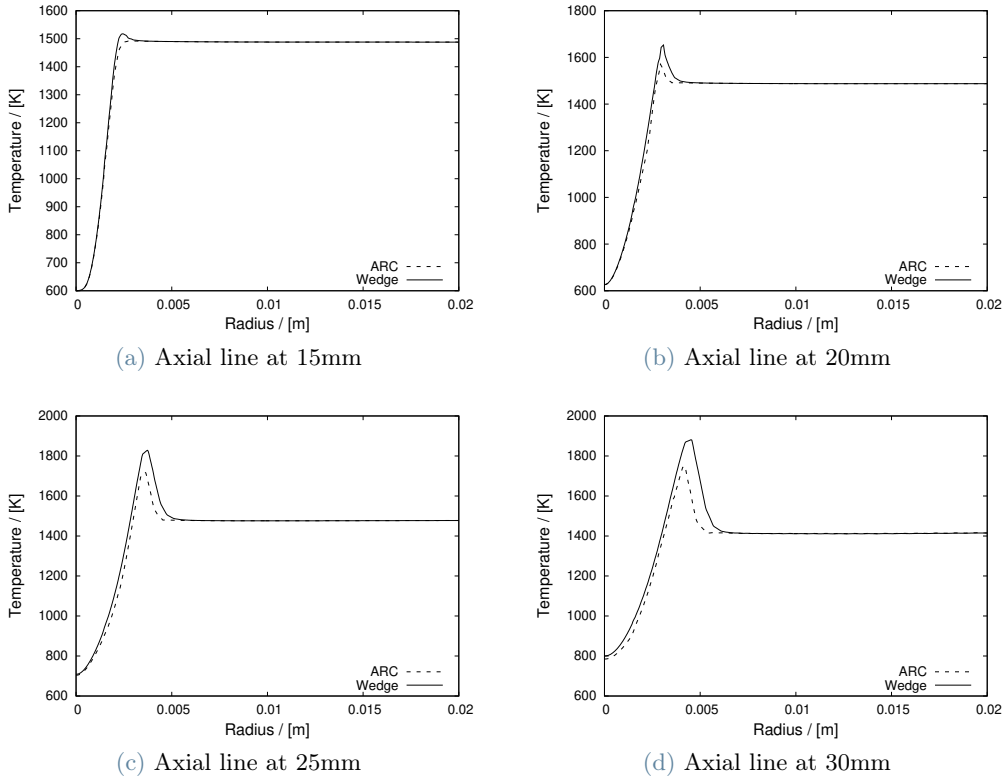


(a) Axial line at 15mm

(b) Axial line at 20mm

(c) Axial line at 25mm

(d) Axial line at 30mm

Figure 16: Temperature comparison: classic approach vs ARC approach

A more detailed investigation about the arc results is proposed in Fig. (17), where the chemistry species and reactions of the simulation have been plot. In Fig. (17a) the number of different species over time is reported, showing a maximum of 22 active species. This means that not many species can be treated as QSS. In fact, the number of QSS species goes from 5 in the first part of the simulation to 4 during the last timesteps.
A reactions analysis has been done as well, with a maximum number of active reactions equal to 122. In Fig. (17c) this analysis is reported: in the first part of the simulation 26 QSS reactions are found, with a decrease during the last part of the simulation, where the QSS reactions go to 17. This behavior reflects the exact trend of the species behavior. In the sub-analysis of the QSS reactions, presented in Fig. (17d), only one reaction has two QSS, the remaining 25 reactions are characterized by the presence of a single QSS reaction. When the QSS reactions decrease and reach 17, only single QSS reactions are present in the simulation.

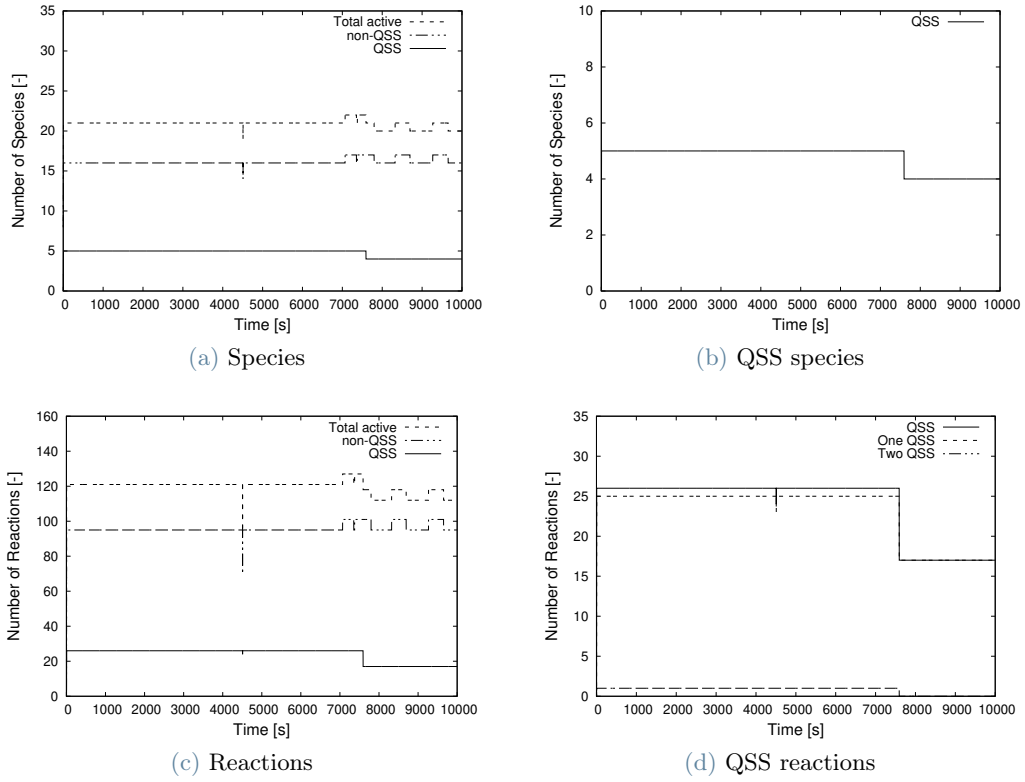


(a) Species (b) QSS species

(c) Reactions (d) QSS reactions

Figure 17: ARC: species and reactions details

In the last part of this simulation, a time comparison has been presented. The Fig. (18) shows on the x axis the simulation timestep, while on the y axis, the execution time obtained. As before, the graph reports the comparison between the two studied approaches underlying a final speedup of the ARC approach of about 8%, reflecting an advantage in calculation time, bringing to a save of the computational effort. It is important to highlight that, in the first part of the simulation, the two computational times are almost the same, with negligible differences.

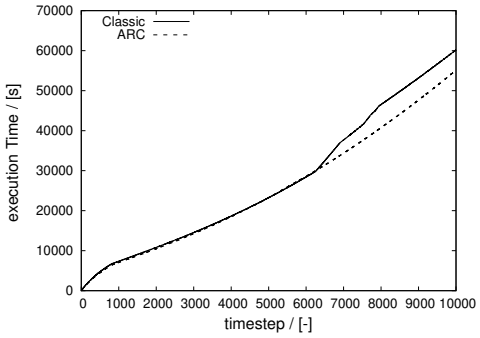


Figure 18: Execution Time Comparison

# 3. High momentum jet flames at elevated pressure

The third case developed in the thesis is focused on the study of flame structures and combustion reactions of a high momentum jet flame.
This case is taken from [31] where a gas turbine burner based on the FLOX® burner concept is developed. The main design feature of these type of concepts are circular arranged nozzles for a partially premixed air and fuel mixture that enters the combustion chamber with high momentum. This leads to a zone where an inner recirculation zone is present and here hot burned gases are transported upstream to generate ignition and stabilization of the flame thanks to strong turbulent mixing with the unburned fresh gas.

## 3.1. Experimental setup

The experimental setup is developed at the high pressure combustion test rig of the DLR Institute of Combustion Technology. The combustion chamber and the burner are placed inside the pressure casing for the tests. The combustion chamber has a square cross section of 95 x 95 $mm^2$ and a length of 843 mm from the burner plate to the exhaust gas nozzle.
The single nozzle of the burner main stage consists of a tube with a 40 mm diameter. A multi-fuel injector is located 400 mm upstream from the nozzle exit.
The fuel injector is constituted by 7 individual pilot nozzles placed in a row and inclined by 60° towards the main stage. The mixing duct that enhances the turbulent mixing between fuel and air is placed with its axis out of the center of the base plate by 10 mm.

Fig. (19) and Fig. (20) show a rapresentation of the described combustion chamber and its details.

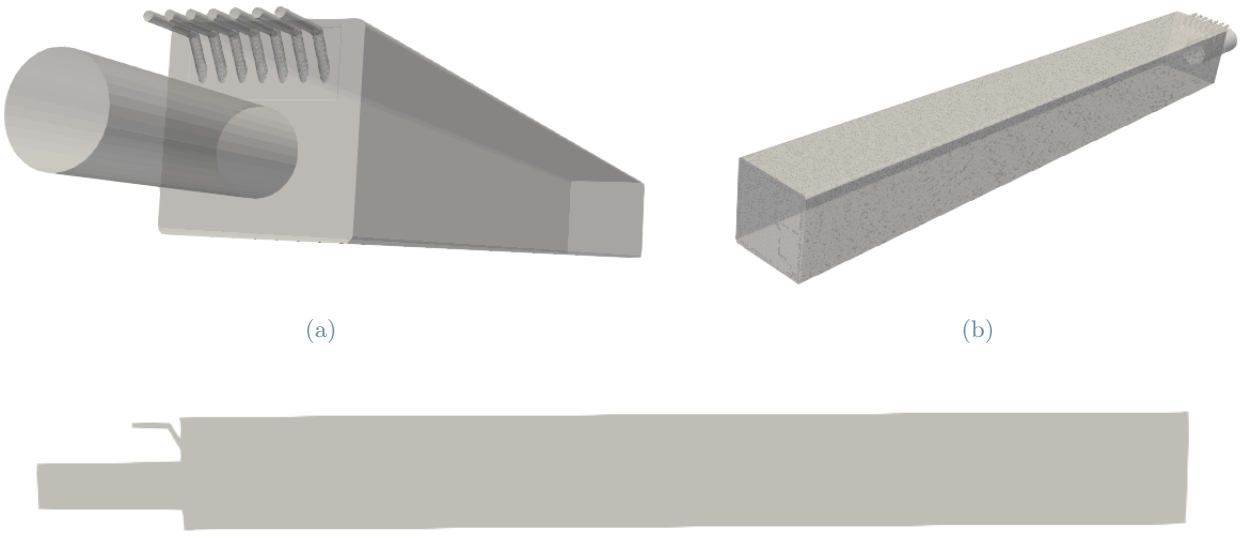

(a) (b)

(c)

Figure 19: Combustion chamber geometry

In the described setup the optically accessible area is given through a window of 88 x 160 $mm^2$ which is the area of the combustion chamber where all experimental results are developed. The accessible area of the combustion chamber is reported graphically in Fig. (21).
In the experimental work, two different cases have been developed: a) a case with an unpiloted flame development; b) a case with a piloted flame development. In this study, the first scenario has been investigated, characterized by the operating conditions reported in Tab. (4).

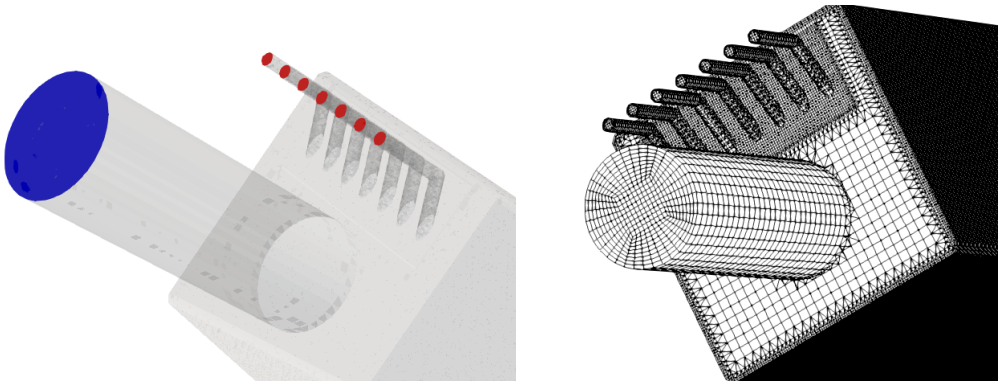

(a) Air inlet in blue, methane inlets in red (b) Mesh discretization

Figure 20: inlet details

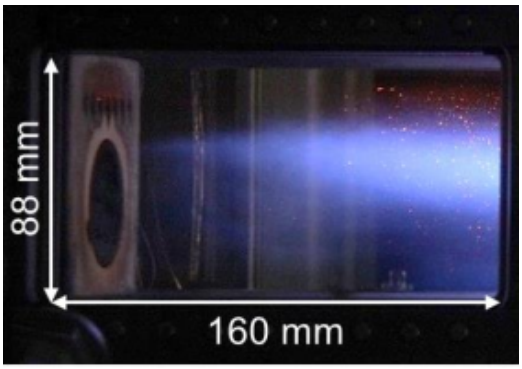


Figure 21: Optically accessible area

| Quantity | Field | Units | Value |
|---|---|---|---|
| Pressure | p | (bar) | 8 |
| Adiabatic flame temperature | $T_{ad}$ | (K) | 1900 |
| Global air-fuel equivalent ratio | $\lambda$ | | 1.83 |
| **Main burner** | | | |
| Jet velocity | $v_{jet}$ | (m/s) | 111 |
| Preheat temperature | $T_{air}$ | (K) | 725 |
| **Pilot burner** | | | |
| Jet velocity | $v_{jet}$ | (m/s) | - |
| Preheat temperature | $T_{air}$ | (K) | - |

Table 4: Unpiloted flame operating conditions

The initial and boundary conditions are set accordingly to make a comparison with the unpiloted flame case, as shown in Tab. (5).

| Region | Field | Description | Type | Value | Units |
|---|---|---|---|---|---|
| **Internal field** | p | Pressure | uniform | 8e5 | Pa |
| | T | Temperature | uniform | 725 | K |
| | $\omega$ | Turbulent mixing length frequency inlet | uniform | 1e-5 | $s^{-1}$ |
| | k | Turbulent intensity kinetic energy inlet | uniform | 1e-4 | $m^2/s^2$ |
| | $Y_{O_2}$ | Oxygen mass fraction | uniform | 0.23 | - |
| | $Y_{N_2}$ | Nitrogen mass fraction | uniform | 0.77 | - |
| **Burner inlet** | U | Velocity | fixedValue | 111 | m/s |
| | T | Temperature | fixedValue | 725 | K |
| | k | Turbulent intensity kinetic energy inlet | uniform | 0.05 | $m^2/s^2$ |
| | $\omega$ | Turbulent mixing length frequency inlet | uniform | 0.02 | $s^{-1}$ |
| | k | Turbulent kinetic energy | uniform | 0.05 | - |
| | $Y_{CH_4}$ | Methane mass fraction | fixedValue | 0.0305 | - |
| | $Y_{O_2}$ | Oxygen mass fraction | fixedValue | 0.204 | - |
| | $Y_{N_2}$ | Nitrogen mass fraction | fixedValue | 0.7655 | - |

Table 5: Initial and boundary conditions unpiloted flame case

## 3.2. Numerical setup

As anticipated in the previous chapters, the main aim of this work to develop a method that brings advantages under two aspects: computational cost and time saving. For this reason it has been implemented the QSSA method that, for a correct analysis, has been compared with a 'classic' approach.
Numerically, for the 'classic' approach the High momentum jet flames case has been set to reflect in the most accurate way the experimental setup.
A brief explanation of the main choices is presented. The Eddy Dissipation Concept (EDC) model (described in section 1.3.1) is chosen as combustion model. In particular, the 2005 version of the EDC has been imposed, together with its own parameters (see Tab. (6)).

| **Coefficients** | $C_1$ | $C_2$ | $C_\gamma$ | $C_\tau$ |
|---|---|---|---|---|
| **Value** | 0.05774 | 0.5 | 2.1377 | 0.4083 |

Table 6: EDC model coefficients

The nature of the experiment identifies the presence of turbulence which brings to set a $k-\omega$ Shear Stress Transport (SST) model. This model is able to capture flow separation and to overcome the deficiencies of the standard $k-\omega$ model with respect to dependency on the freestream values of k and $\omega$ [32], [13]. The model provides two equation for the turbulence kinetic energy k and turbulence specific dissipation rate $\omega$. Model equations and default coefficients are treated in Appendix B.
The described model works as a precursor of the Large Eddy Simulation (LES) model (which uses the turbulent kinetic energy equation), typically adopted in transient 3D cases.
Regarding the chemistry two different approaches have been used: the ODE solver already implemented in OpenFOAM® and the QSSA developed model. In both cases an implicit ODE solver, the Seulex one, has been tested.

In the present case, numerical schemes for involved terms have been set in the fvSchemes dictionary in the system directory. The first order Euler (bounded and implicit) scheme has been selected to handle time derivatives. A second order Gauss integration scheme is instead used for the gradient terms, as well as for the laplacian scheme. In particular, for the latter, a Gauss linear orthogonal scheme is picked.

In the dictionary that set the schemes required for the handling of divergence operations a second order, unbounded, Gauss limitedLinear scheme has been selected for all terms, except for two terms: the two divergences that involve k and $\omega$ which have a first order, bounded, Gauss upwind scheme.
Last, the reactingFoam application solver has been used in the simulation, as anticipated in section 1.5. The simulation has been set to last 0.5 seconds, with a $\Delta t$ equal to 1e-7 s and a maximum Courant number fixed to 0.2. In these simulations the timestep is low because the chemistry is predominant over the fluid dynamics and the maximum Courant number have to assume a low value to ensure stability and convergence to the solution.

## 3.3. Results

### 3.3.1 Comparison between simulation and experimental results

In the following section, the results of the comparison between experiment and simulation are presented. Firstly, for the comparison, the velocity trend in the internal region of the chamber has been analysed in Fig. (22). In Fig. (22a) the resultant velocity of the experiment is shown and the analysed region corresponds to the optically accessible area of the chamber, while, on the right side (Fig. (22b)), the simulation velocity is reported, analysed on a chamber extension equal to the experimental one.
In this comparison, a good match of the velocity values is present and a strong similarity between the development of the two regions is shown. However, it can be noticed a small difference of the velocity distribution, which, in the simulation case, has a larger elongation both on x and y axis.
The flow has a correct qualitative behavior, a fundamental characteristic for further studies, because in the upper part of the chamber, a recirculation zone is present. The recirculation zone has a key role in the study of the piloted case because it can improve the mixing between fuel and air and, as consequence, probably generating a good comparison with the experiment case.

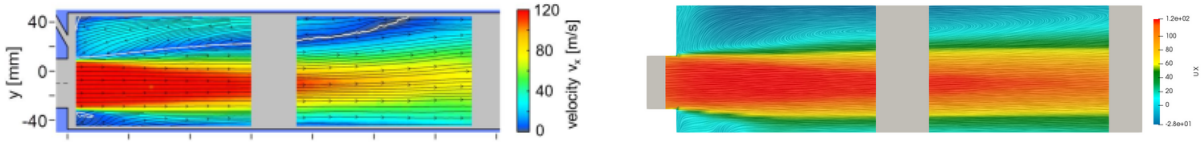


(a) Sperimental velocity (b) Simulation velocity

Figure 22: Velocity Comparison

To better understand the behavior of the simulation, an analysis of the chemical species, such as the $CH_4$ and the $H_2O$, has been studied. In Fig. (23, 24) the concentration distribution of the two species is compared with the experimental one. Both the images show a similar trend: the concentration development has the same behavior with the experimental one, with a good match of the concentration values, but, also in this case, the elongation of the intermediate portion of the species is bigger than the experimental one.
One possible reason to this mismatch, is the adopted combustion model: in the simulation, the advection-diffusion equations, responsable of the chemical species evolution, are influenced by the reaction rate ($\dot{\omega}$) of the combustion model. So, if the reaction rate is not the same of the experimental one, the chemical species have a different evolution and elongation. This elongation could be fixed with a different tuning of the combustion model and of his coefficients but this is not of interest of the thesis.

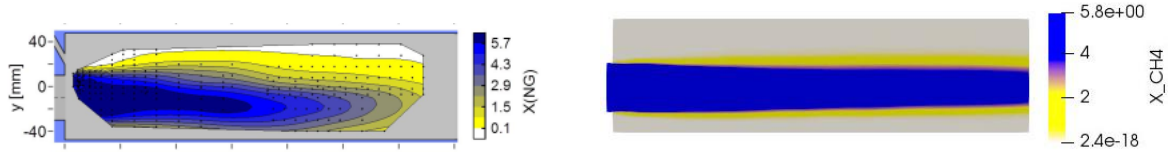


(a) Sperimental $X_{CH4}$ (b) Simulation $X_{CH4}$

Figure 23: CH4 Concentration Comparison

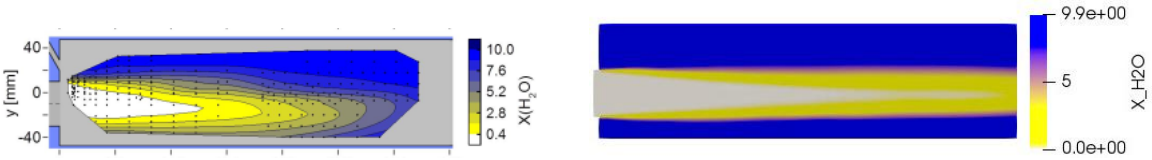


(a) Sperimental $X_{H2O}$ (b) Simulation $X_{H2O}$

Figure 24: H2O Concentration Comparison

In Fig. (25) three different views of the combustion chamber are shown. These images highlight the elongation of the variables and, in particular, in Fig. (25c) it can be noticed the evolution of the temperature that reflects the behavior of the velocity and species concentration.

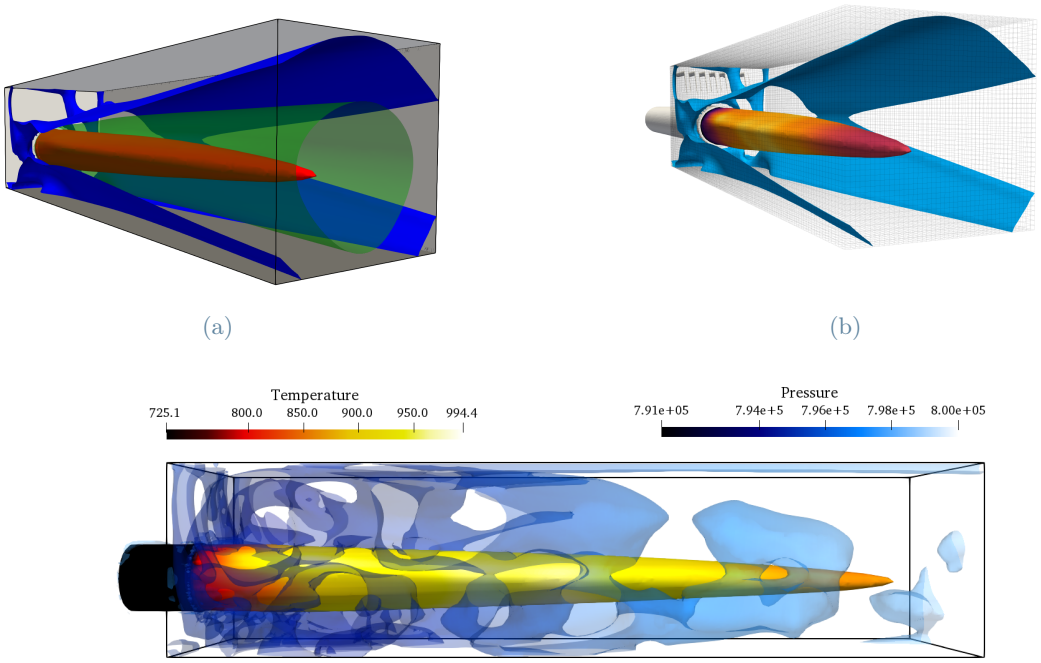


(a) (b)

(c) Temperature and Pressure evolution

Figure 25: 3D Views: evolution of species concentration, temperature and pressure

### 3.3.2 Comparison between classical approach and ARC approach

In this section, a comparison between classical approach and ARC approach is presented.
The ARC simulation has been run with the same setting of the first case (Sec. 3.3), with a Local Time Stepping (LTS) method because of the difficulty to run the ARC simulation with the Euler time scheme. The simulation has been run up to steady state, overcoming the transient, to have a meaningful comparison between the two approaches. The validation has been run with multiple tolerances, finding a good trade-off between accuracy and QSS species and reactions present, with a value of 1e-7 for the maxTolQSS and a value of 1e-8 for the minTolQSS.
The aim of the comparison is give continuity to Sec. 3.3 one and so, to analyse the temperature profile inside the combustion chamber. Fig. (26) shows four different temperature profiles, each one at a different axial line on the x axis, in particular, at 50mm, 150mm, 250mm and 350mm. In each graph, the continuos line represents the temperature curve of the classic approach while the dotted line the ARC approach one. The figures show similar results between the two approaches, reflecting the results obtained in Sec. 2.5.3, because the temperature profile of the ARC approach follows the trend of the classical one. Numerically, the ARC simulation has different values of T of the order of 125 K, attesting a 6% error, higher with respect to the first case analyzed.
The results of both cases highlight that the ARC approach does not predict in the exact manner the temperature in the hottest zones, which are the zones where the reactions occur. The behavior reflects the QSS approximation nature because it introduces an error which is higher where fast phenomena, such as the combustion, are present.

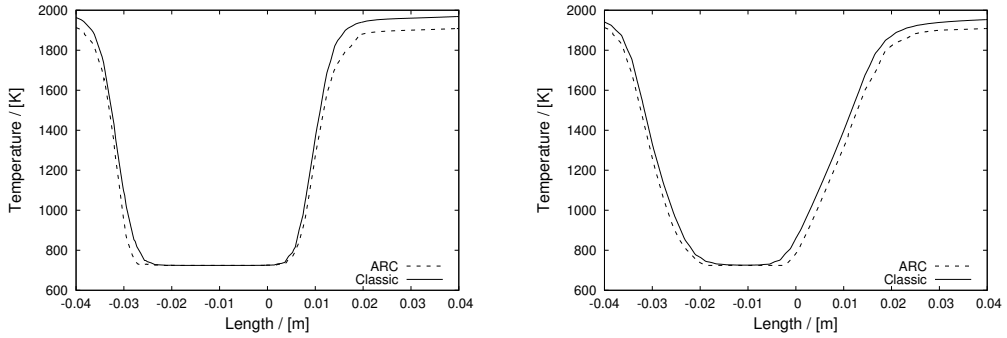


(a) Axial line at 50mm

(b) Axial line at 150mm

(c) Axial line at 250mm

(d) Axial line at 350mm

Figure 26: Temperature comparison: classic approach vs ARC approach

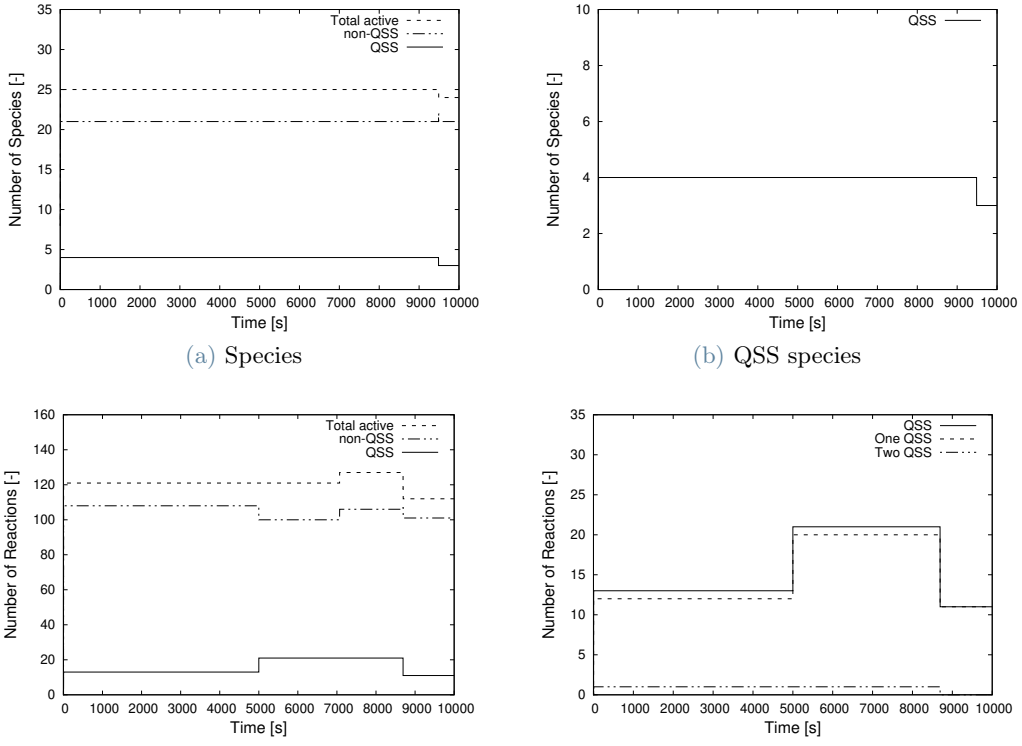


(a) Species

(b) QSS species

(c) Reactions

(d) QSS reactions

Figure 27: ARC: species and reactions details

In Fig. (27) a validation of the QSS species and reactions are shown. In particular, Fig. (27a, 27b) show the QSS detected species over time and it can be noticed that the number of active species, in this case, is 25 with a low number of QSS detected. In fact the QSS species reach a number of 4 to decrease to 3 for the rest of the simulation.

Fig. (27c, 27d) show the number of reactions over time. The number of the total active reactions of the simulation has a maximum of 128 with the QSS reactions that are 22 in total. In the detailed reaction, focusing on the composition of the QSS reactions, it can be noticed that only one reaction has the presence of a double QSS, while in the rest of the simulation, only single QSS reactions are present.

# 4. Conclusions

The 'auto-ignition of a methane jet in a hot coflow' case has been developed. Two different geometries have been built and validated with respect to the experimental results to show the accuracy and reliability. The wedge geometry case and the 3D geometry one have been compared showing the good match of results. Thanks to this, the wedge geometry case has been selected for the validation of the QSS approximation.
The 'high momentum jet flames at elevated pressure' case has been implemented. it has been validated and compared with the experimental results, in particular, with the unpiloted flame development scenario. In this case, such as in the first one, the simulation results have been developed both with the 'classic' chemistry approach and with the QSS approximation. The two results have been compared to show the reliability of the implemented code.
The quasi-steady-state approximation has been implemented and tested. The 'classic' chemistry solution of OpenFOAM has been modified developing the QSS approximation source code. This code has been implemented to select steady state species run-time, with a variable tolerance, with the aim of reducing the ODEs system and introducing an agebraic system. In this way the problem has been characterized by a reduced stiffness and a reduced computational effort. The tolerance function has been developed to change run-time. This allows the tolerance to follow the evolution of the temperature gradient which works with both explicit and implicit simulations. The consideration of the steepness of the temperature gradient allows to obtain more accurate results and a more precise QSS species consideration. The QSS approximation has been tested on the two multi-cell reacting cases: the 'Auto-ignition of a methane jet in a hot coflow' and the 'High momentum jet flames at elevated pressure'.
The results between the 'classic' approach and the ARC approach have been analysed. Both cases show a good approximation of the temperature profile, studied in several axial lines position, with a maximum error of 5% for the first case and of 6% for the second case. Both the simulations have detected the presence of QSS species and reactions. The number of found species is low and this demonstrate that, for further application, a better tuning of the sensitivity parameter and of the level of importance variables can help to speed up further the simulation.

Next steps of this study could focus on improving the precision and the reliability of the QSS approximation, and on maintaining the code for the latest version of OpenFOAM®. At the same time, higher acceleration can be achieved by extending the code to heterogeneous supercomputing. The possible objectives that can be achieved are:

- increase the number of QSS species found through the introduction of new parameters and sensitivity levels;
- test the piloted configuration of the 'high momentum jet flame at elevated pressure' to address the ability of the ARC approach to produce results comparable to the experimental ones;
- validate and confirm the level of accuracy of the QSS approximation with other industrial multi-cell cases, and in combination with the latest version of OpenFOAM®;
- integrate the ARC method with a GPGPU hybrid approach: since the stiffness of the chemical ODE system is reduced by means of the ARC approach, the GPU becomes the favorable choice to perform explicit ODE integration due to its massively parallel architecture.

# References


[1] Cant Stewart. High-performance computing in computational fluid dynamics: progress and challenges. 2002.

[2] Shamoon Jamshed. *The Way the HPC Works in CFD*, pages 41–79. 12 2015.

[3] ExaFOAM, 2022.

[4] Tianfeng Lu and Chung K. Law. Toward accommodating realistic fuel chemistry in large-scale computations. *Progress in Energy and Combustion Science*, 35(2):192–215, 2009.

[5] Thierry Baritaud, Thierry Poinsot, and Markus Baum. *Direct numerical simulation for turbulent reacting flows*. Editions Technip, 1996.

[6] J. C. Sutherland J. H. Chen E. H. Hawkes, R. Sankaran. Direct numerical simulation of turbulent combustion: fundamental insights towards predictive models. *Journal of Physics*, 16, 2005.

[7] Graham M. Goldin, Zhuyin Ren, and Selma Zahirovic. A cell agglomeration algorithm for accelerating detailed chemistry in cfd. *Combustion Theory and Modelling*, 13(4):721–739, 2009.

[8] Tianfeng Lu and Chung Law. Systematic approach to obtain analytic solutions of quasi steady state species in reduced mechanisms. *The journal of physical chemistry. A*, 110:13202–8, 01 2007.

[9] Anne Felden. *Development of Analytically Reduced Chemistries (ARC) and applications in Large Eddy Simulations (LES) of turbulent combustion*. PhD thesis, 2017.

[10] JY Chen. Development of reduced mechanisms for numerical modelling of turbulent combustion. In *Workshop on Numerical Aspects of Reduction in Chemical Kinetics*. CERMICS-ENPC Cite Descartes Champus sur Marne, France, 1997.

[11] Milovan Peric Joel H. Ferziger. *Computational Methods for Fluid Dynamics*. Springer Berlin, Heidelberg.

[12] GitHub, 2022.

[13] The OpenFOAM Foundation.

[14] L.Y.M. Gicquel, G. Staffelbach, and T. Poinsot. Large eddy simulations of gaseous flames in gas turbine combustion chambers. *Progress in Energy and Combustion Science*, 38(6):782–817, 2012.

[15] D. Veynante and T. Poinsot. Reynolds averaged and large eddy simulation modeling for turbulent combustion. In Olivier Metais and Joel H. Ferziger, editors, *New Tools in Turbulence Modelling*, pages 105–140, Berlin, Heidelberg, 1997. Springer Berlin Heidelberg.

[16] Zhiyi Li, Marco Ferrarotti, Alberto Cuoci, and Alessandro Parente. Finite-rate chemistry modelling of non-conventional combustion regimes using a partially-stirred reactor closure: Combustion model formulation and implementation details. *Applied Energy*, 225:637–655, 2018.

[17] M. T. Landahl and E. Mollo-Christensen. *Turbulence and Random Processes in Fluid Mechanics*. Cambridge University Press, Cambridge, 2 edition, 1992.

[18] B. F. Magnussen. The eddy dissipation concept a bridge between science and technology. 2005.

[19] P. Pepiot, H. Pitsch, and Stanford University. Department of Mechanical Engineering. *Automatic Strategies to Model Transportation Fuel Surrogates*. Stanford University, 2008.

[20] Daniel Nilsson. *Automatic Analysis and Reduction of Reaction Mechanisms for Complex Fuel Combustion*. PhD thesis, Lund University, 2001.

[21] T. Løvas, A. Løvas, Per, Mauss, Fabian, and Mastorakos. Comparison of automatic reduction procedures for ignition chemistry. 2002.

[22] J.-Y. Chen. Automatic generation of reduced mechanisms and their applications to combustion modeling. *Trans. Aero. Astro. Soc. Rep. China*, 2001.

[23] C. J. Montgomery, M. A. Cremer, J.-Y. Chen, C. K. Westbrook, and L. Q. Maurice. Reduced chemical kinetic mechanisms for hydrocarbon fuels. *J. Prop. Power*, 2002.

[24] T. Turányi, A. S. Tomlin, , and M. J. Pilling. On the error of the quasi-steady state approximation. *J. Phys. Chem*, 1993.

[25] Tamás Turányi. Applications of sensitivity analysis to combustion chemistry. *Reliability Engineering and System Safety*, 57(1):41–48, 1997.

[26] T. Løvas, D. Nilsson, and F. Mauss. Automatic reduction procedure for chemical mechanisms applied to premixed methane/air flames. *Proceedings of the Combustion Institute*, 28(2):1809–1815, 2000.

[27] A. Fiolitakis and C. M. Arndt. Transported pdf simulation of auto-ignition of a turbulent methane jet in a hot, vitiated coflow. *German Aerospace Center, Stuttgart, Germany*, 2019.

[28] C.M. Arndt, R. Schießl, J.D. Gounder, W. Meier, and M. Aigner. *Flame stabilization and auto-ignition of pulsed methane jets in a hot coflow: Influence of temperature.* Proc. Combust. Inst., 2013.

[29] B. E. Launder and D. B. Spalding. The numerical computation of turbulent flows. computer methods in applied mechanics and engineering. pages 269–289, 1974.

[30] S. H. El Tahry. k-epsilon equation for compressible reciprocating engine flows. *Journal of energy*, pages 345–353, 1983.

[31] Holger Ax, Oliver Lammel, Rainer Luckerath, and Michael Severin. High-momentum jet flames at elevated pressure, c: Statistical distribution of thermochemical states obtained from raman measurements. *Journal of Engineering for Gas Turbines and Power*, 2020.

[32] Florian Menter, M. Kuntz, and RB Langtry. Ten years of industrial experience with the sst turbulence model. *Heat and Mass Transfer*, 4, 01 2003.

# A. Appendix A: Jacobian and chemical time

The Jacobian matrix can be related to the rate of change of species source terms when there is a change in species concentrations. Analogously, an inverted Jacobian element can represent as a characteristic time scale for a species.
A demonstration of this relationship is proposed in this appendix.
Assume a system of first order, non linear, ordinary differential equations composed as:

$$\frac{dy}{dt} = f(y(p,t),p) \tag{37}$$

with f as a source term of the variable y dependent on time and on constant parameter p.
Differentiation both sides with respect to p yelds:

$$\frac{d}{dp}(\frac{dy}{dt}) = \frac{d}{dp}(f(y(p,t),p) \tag{38}$$

Expanding both sides, the final expression becomes:

$$\frac{\partial}{\partial t}(\frac{\partial y}{\partial p}) = \frac{\partial f}{\partial y}\frac{\partial y}{\partial p} + \frac{\partial f}{\partial p} \tag{39}$$

Identifying the Jacobian matrix as $J = \frac{\partial f}{\partial y}$ it can be obtained a set of differential equations for a generally sensitivity matrix $S = \frac{\partial f}{\partial p}$ determined by the system:

$$\frac{\partial S}{\partial t} = JS + \frac{\partial f}{\partial p} \tag{40}$$

with a forcing term $\frac{\partial f}{\partial p}$.

A chemical system has the caractheristic to be strongly non linear and it has to be linearized around a point $y_0$ in state space. This linearization brings to:

$$\frac{d}{dt}(y - y_0) = f_0 + J(y - y_0) \tag{41}$$

where $y_0$ is constant in time.

This can be represent a linearized state representation of eq. 37 in the most general form:

$$\frac{dy}{dt} = Jy + Bw \tag{42}$$

with a constant input signal $w = f_0 - jy_0$ and B equal to the unity matrix.
The general solution of the linearized system is:

$$y(t) = e^{J(t-t_0)}y(t_0) + \int_{t_0}^{t} e^{J(t-\tau)}Bw(\tau)d\tau \tag{43}$$

The Jacobian matrix here is assumed to be diagonalizable and for this $e^J$ is defined as:

$$e^J = Qe^{\Lambda}Q^{-1} \tag{44}$$

where $\Lambda$ is the diagonal ,atrix of eigenvalues of J.
If J is a constant system matrix for a linear system, one has:

$$J = QTQ^{-1} = QTQ^T \tag{45}$$

and the ODE system can be written:

$$\frac{dy}{dt} = QTQ^Ty \tag{46}$$

Setting a change of variables: $\hat{y} = Q^Ty$ and inserting eq. 45, one obtain:

$$\frac{d}{dt}Q\hat{y} = QTQ^TQ\hat{y} = QT\hat{y} = QQ^TJQ\hat{y} \tag{47}$$

which multiplying by $Q^T$, becomes:

$$\frac{d\hat{y}}{dt} = Q^T J Q \hat{y} \tag{48}$$

By choosing a transformation which yelds eigenvalues $\lambda_i$ in dwscwnding order along the diagonal of T, the new system matrix is:

$$Q^T J Q = \begin{pmatrix} J'_{11} & J'_{12} \\ 0 & J'_{22} \end{pmatrix} \tag{49}$$

with $J'_{11}$ connected to the most negative eigenvalues and so to the fastest relaxing modes, and $J'_{22}$ corresponding to the slowest modes.
Expressing now y(t):

$$y(t) = e^{J(t-t_0)} y(t_0) + \int_{t_0}^{t} e^{J(t-\tau)} (f_0 - J y_0) d\tau \tag{50}$$

Setting $y(t_0) = y_0 + \Delta y_0$, where $\Delta y_0$ is a perturbation of the initial concentration vector $y(t_0)$, the integration for a single species i is:

$$\begin{aligned} y_i(t) &= ((y_0)_i + (\Delta y_0)_i) e^{J_{ii}(t-t_0)} + [((f_0)_i - J_{ii}(y_0)_i) \frac{-1}{J_{ii}} e^{J_{ii}(t-\tau)}]_{t_0}^{t} = \dots \\ &= (f_0)_i + (\Delta y_0)_i e^{J_{ii}(t-t_0)} - \frac{-1}{J_{ii}} (f_0)_i (1 - e^{J_{ii}(t-t_0)}) \end{aligned} \tag{51}$$

Differentiation with respect to t and insertion of $t_0$ gives the rate of change of species i due to addition of $(\Delta y_0)_i$ around the linearization point:

$$\frac{dy_i}{dt}(t_0) = (f_0)_i + J_{ii} (\Delta y_0)_i \tag{52}$$

This would indicate that jacobian diagonal element $J_{ii}$ measures the rate of relaxation of $y_i$ towards the original state, and accordingly that $-1/J_{ii}$ is a measure of the corresponding relaxation time that in the present work is the characteristic chemical time.

# B. Appendix B: Model equations and default coefficients of kOmegaSST turbulence model

The turbulence specific dissipation rate equation is given by:

$$\frac{D}{Dt}(\rho\omega) = \nabla \cdot (\rho D_\omega \nabla\omega) + \frac{\rho\gamma G}{\nu} - \frac{2}{3}\rho\gamma\omega(\nabla \cdot u) - \rho\beta\omega^2 - \rho(F_1 - 1)CD_{k\omega} + S_\omega \tag{53}$$

and the turbulence kinetic energy by:

$$\frac{D}{Dt}(\rho k) = \nabla \cdot (\rho D_k \nabla k) + \rho G - \frac{2}{3}\rho k(\nabla \cdot u) - \rho\beta^*\omega k + S_k \tag{54}$$

The turbulence viscosity is obtained using:

$$\nu_1 = a_1 \frac{k}{max(a_1\omega b_1 F_{23} S)} \tag{55}$$

The default coefficients of the model are presented in tab. (7):

| **Coefficients** | $a_{k1}$ | $a_{k2}$ | $a_{\omega 1}$ | $a_{\omega 2}$ | $\beta_1$ | $\beta_2$ | $\gamma_1$ | $\gamma_2$ | $\beta^*$ | $a_1$ | $b_1$ | $c_1$ |
|---|---|---|---|---|---|---|---|---|---|---|---|---|
| **Value** | 0.85 | 1.0 | 0.5 | 0.856 | 0.075 | 0.0828 | 5/9 | 0.44 | 0.09 | 0.31 | 1.0 | 10.0 |

Table 7: kOmegaSST model coefficients

# Abstract in lingua italiana

La comunità industriale ha accresciuto recentemente l'interesse nell'implementazione e nell'ottimizzazione degli algoritmi per la Fluidodinamica Computazionale (CFD). Questo elaborato investiga l'uso dell'approccio Analitically Reduced Chemistry (ARC) per trovare una soluzione rapida ai problemi con fluidi reattivi in casi Aerospaziali, preservando un'accuratezza accettabile dei risultati. L'approssimazione Quasi-Steady State (QSS) è stata implementata e testata per trattare le specie con un basso ciclo vita e concentrazioni come steady state. Le specie QSS sono state selezionate anche grazie ad un coefficiente di sensibilità secondo un approccio chiamato Level of Importance (LOI), per poi includere nella lista QSS le specie con un lungo ciclo vita ma bassa sensibilità. Un sistema algebrico di equazioni aggiorna la concentrazione delle specie QSS riducendo il costo dell'integrazione delle ODE. Questo aiuta a ridurre la stiffness del sistema del sistema di ODE della chimica, promuovendo un'accelerazione della sua soluzione. L'uso del metodo di eliminazione (DAC) accelera maggiormente le simulazioni dei meccanismi chimici. La validazione è stata effettuata su due casi. Le simulazioni sono state condotte tramite il software CFD OpenFOAM®. Sono stati considerati due modelli di combustione: l'Eddy Dissipation Concept (EDC) e il Partially Stirred Reactor (PaSR). Le soluzioni sono state validate con i risultati sperimentali presenti in letteratura.

**Parole chiave:** OpenFOAM, CFD, Jet in Hot Coflow, High Momentum Jet Flame, QSS Approximation, Analitically Reduced Chemistry